Geophysical Journal International

Geophys. J. Int. (2011) **187,** 705–728 doi: 10.1111/j.1365-246X.2011.05203.x

Sensitivity of controlled-source electromagnetic fields in planarly layered media

R. Streich[1,2] and M. Becken[3]

[1] *GFZ German Research Centre for Geosciences, Telegrafenberg,* 14473 *Potsdam, Germany. E-mail: rstreich@gfz-potsdam.de*
[2] *Institute of Earth and Environmental Science, Potsdam University, Karl-Liebknecht-Str.* 24, 14476 *Potsdam-Golm, Germany*
[3] *Institute of Geophysics, University of Münster, Corrensstraße* 24, 48149 *Münster, Germany*

Accepted 2011 August 24. Received 2011 August 24; in original form 2011 January 26

SUMMARY

The study of electromagnetic (EM) field sensitivities is useful for assessing the feasibility of controlled-source electromagnetic (CSEM) surveys. Sensitivity calculations are also a principal building block of EM inversion schemes. Sensitivities are formally given by the derivatives of the EM field components with respect to conductivity. For horizontally layered media, these derivatives can be evaluated analytically, offering advantages in computational efficiency and accuracy over numerical evaluation. We present a complete set of explicit analytic expressions for the EM field sensitivities in 1-D VTI-anisotropic media for horizontal and vertical electric and magnetic dipole sources, and also for finite horizontal electric sources. Since our derivations are based on a formulation for EM fields that is quite general in allowing for sources and receivers at any depth, our sensitivity expressions exhibit the same generality. We verify our expressions by comparison to numerical solutions, and finally present application examples that demonstrate the utility and versatility of these expressions for CSEM feasibility studies.

Key words: Electromagnetic theory.

1 INTRODUCTION

Nearly a decade ago, controlled-source electromagnetics (CSEM) was optimistically viewed as a potential method for direct hydrocarbon indication (Eidesmo *et al.* 2002). Such enthusiasm, though, was soon followed by the insight that more thorough understanding of electromagnetic (EM) field phenomena is required to assess the capabilities and limitations of the method when applied in geologically complex settings. Accordingly, efforts were strengthened to investigate EM field behaviour (Constable & Weiss 2006; Um & Alumbaugh 2007; Weidelt 2007; Andréis & MacGregor 2008; Key 2009; Orange *et al.* 2009; Chave 2009; Løseth 2011) and assess the resolution capabilities of CSEM in various environments (Abubakar *et al.* 2010; Streich *et al.* 2010; Wirianto *et al.* 2010).

One tool that can be used for studying CSEM feasibility is the analysis of sensitivities, formally expressed as the derivatives of EM field components with respect to the conductivity of subsurface structures (e.g. layers or blocks). The same evaluation of sensitivities is also an essential part of EM inversion algorithms. In both cases, rapid and accurate computation of sensitivities for many source–receiver pairs is required.

Sensitivities can be calculated numerically using finite-difference or other numerical differentiation techniques. However, since the dependency between EM fields and conductivity is non-linear, straightforward finite-difference evaluations of sensitivity may be inaccurate, and approaches that exhibit higher-order accuracy may be computationally expensive. For planarly layered media, sensitivity can also be calculated analytically, which should generally be more efficient and more accurate than numerical evaluation. In addition, analytic expressions may provide insights into EM field behaviour that are not apparent from numerical computations.

In many cases, conductivity is assumed to be approximately isotropic or VTI-anisotropic (i.e. horizontal and vertical conductivities differ; Everett & Constable 1999; Newman *et al.* 2010). Then, similar to the EM field components themselves, their derivatives can be expressed in terms of Bessel function integrals. These can be rapidly evaluated using fast Hankel transform filters (e.g. Johansen & Sørensen 1979; Anderson 1982; Christensen 1990), thus providing sensitivities with a computational effort comparable to that required for calculating the EM fields.

Although recent algorithmic developments in combination with high-end computer hardware now facilitate considering 3-D conductivity structure (Haber *et al.* 2007; Commer & Newman 2008; Zhdanov 2009), investigation of layered media is important for studying first-order effects, initial data interpretation, or generation of starting models for higher-dimensional inversion. Layered-media sensitivities have also

been used for approximate Jacobi matrix calculation within 3-D inversion algorithms (Farquharson & Oldenburg 1996; Newman & Boggs 2004).

The analytic calculation of layered-media sensitivities is straightforward in principle, as was shown by Chave (1984); Flosadóttir & Constable (1996); Key (2009). We extend this previous work by presenting explicit expressions for sensitivities due to electric and magnetic dipole sources at arbitrary orientation and depth within the layer stack, for receivers that may also be located at any depth. In addition, we derive explicit sensitivities for long horizontal wire sources. This presentation of full analytical expressions should be useful for reference, and beneficial for readers implementing EM modelling and inversion algorithms. We start our derivations from the VTI-anisotropic version of the EM field expressions presented by Løseth & Ursin (2007), and extensions thereof for sources of finite extent (Streich & Becken 2011). We then present complete expressions for the various source types, and briefly describe the reduction to isotropic media in the appendix. To verify our formulas, we compare them to EM field derivatives obtained by numerical differentiation, using a typical marine CSEM model. Finally, we present applications for studying the feasibility of land-based CSEM exploration and monitoring of thin resistive and conductive layers.

2 MODEL DESCRIPTION

We consider the layered model geometry depicted in Fig. 1. The z axis is positive downward and the properties of the jth layer are written as

$$\tilde{\varepsilon}_j = d \begin{pmatrix} \varepsilon_{hj} & 0 & 0 \\ 0 & \varepsilon_{hj} & 0 \\ 0 & 0 & \varepsilon_{vj} \end{pmatrix} + \frac{\mathrm{i}}{\omega} \begin{pmatrix} \sigma_{hj} & 0 & 0 \\ 0 & \sigma_{hj} & 0 \\ 0 & 0 & \sigma_{vj} \end{pmatrix},$$

with horizontal and vertical conductivities σ_{h_j} and σ_{v_j}, permittivities ε_{h_j} and ε_{v_j}, angular frequency $\omega = 2\pi f$ and $\mathrm{i} = \sqrt{-1}$. A time dependency $e^{-\mathrm{i}\omega t}$ is assumed. Permittivities are small compared to the conductivity term, but are not neglected to keep the expressions general, and because this allows us to work with true medium properties in air. Magnetic permeability is set to the free-space value μ_0.

In planarly layered media, Maxwell's equations permit a decomposition of the EM field into tangential electric (TE) and tangential magnetic (TM) mode fields (e.g. Ward & Hohmann 1987). The TE and TM mode upward and downward interface reflection and transmission coefficients at the jth layer boundary are found as (Løseth & Ursin 2007, see also Fig. 1)

$$\acute{r}_j^{TE} = \frac{p_{z_{j+1}}^{TE} - p_{z_j}^{TE}}{p_{z_{j+1}}^{TE} + p_{z_j}^{TE}}, \quad \grave{r}_j^{TE} = -\acute{r}_j^{TE}, \quad \acute{t}_j^{TE} = \frac{2\sqrt{p_{z_{j+1}}^{TE} p_{z_j}^{TE}}}{p_{z_{j+1}}^{TE} + p_{z_j}^{TE}}, \quad \grave{t}_j^{TE} = \acute{t}_j^{TE}, \tag{1a}$$

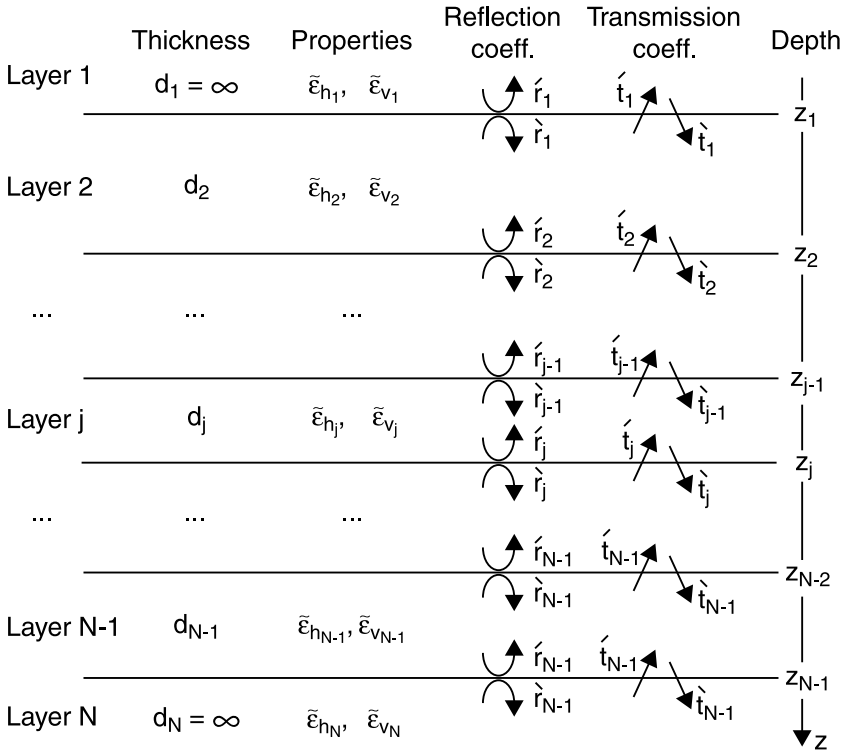

Figure 1. Sketch of the 1-D geometry considered, also showing the indexing of layers and reflection and transmission coefficients.

$$\acute{r}_j^{TM} = \frac{\tilde{\varepsilon}_{h_{j+1}} p_{z_j}^{TM} - \tilde{\varepsilon}_{h_j} p_{z_{j+1}}^{TM}}{\tilde{\varepsilon}_{h_{j+1}} p_{z_j}^{TM} + \tilde{\varepsilon}_{h_j} p_{z_{j+1}}^{TM}}, \quad \grave{r}_j^{TM} = -\acute{r}_j^{TM}, \quad \acute{t}_j^{TM} = \frac{-2\sqrt{\tilde{\varepsilon}_{h_j} p_{z_{j+1}}^{TM} \tilde{\varepsilon}_{h_{j+1}} p_{z_j}^{TM}}}{\tilde{\varepsilon}_{h_j} p_{z_{j+1}}^{TM} + \tilde{\varepsilon}_{h_{j+1}} p_{z_j}^{TM}}, \quad \grave{t}_j^{TM} = \acute{t}_j^{TM}, \tag{1b}$$

with the frequency-normalized vertical wavenumbers (which have the physical unit of slowness)

$$p_{z_j}^{TE} = \sqrt{\tilde{\varepsilon}_{h_j}\mu_0 - p_h^2}, \quad p_{z_j}^{TM} = \sqrt{\tilde{\varepsilon}_{h_j}\mu_0 - \frac{\tilde{\varepsilon}_{h_j}}{\tilde{\varepsilon}_{v_j}} p_h^2},$$

and normalized horizontal wavenumber $p_h = \kappa/\omega = \sqrt{k_x^2 + k_y^2}/\omega$.

3 EM FIELDS IN LAYERED MEDIA

For a consistent and self-contained discussion of EM field derivatives, we repeat here the VTI-anisotropic versions of the EM field expressions from Løseth & Ursin (2007). We also provide VTI-anisotropic versions of the expressions for long horizontal wire sources from Streich & Becken (2011) using exactly the same notation.

3.1 Horizontal electric dipole source

We consider, without loss of generality, a horizontal electric dipole (HED) source located at $(x, y) = (0, 0)$ and oriented in the x direction. The EM field components for such a source and a receiver located at (x, y, z) in an isotropic medium are

$$E_r = -\frac{Il_x}{4\pi}\cos\beta\left[I_{A0}^{TM} + \frac{1}{r}\left(I_{A1}^{TE} - I_{A1}^{TM}\right)\right], \tag{2a}$$

$$E_\theta = -\frac{Il_x}{4\pi}\sin\beta\left[-I_{A0}^{TE} + \frac{1}{r}\left(I_{A1}^{TE} - I_{A1}^{TM}\right)\right], \tag{2b}$$

$$E_z = \frac{Il_x}{4\pi}\frac{i\cos\beta}{\omega\tilde{\varepsilon}_{v_R}}\int_0^\infty \kappa^2 J_1(\kappa r) g_D^{TM}\,\mathrm{d}\kappa, \tag{2c}$$

$$H_r = \frac{Il_x}{4\pi}\sin\beta\left[-I_{D0}^{TE} + \frac{1}{r}\left(I_{D1}^{TE} - I_{D1}^{TM}\right)\right], \tag{2d}$$

$$H_\theta = -\frac{Il_x}{4\pi}\cos\beta\left[I_{D0}^{TM} + \frac{1}{r}\left(I_{D1}^{TE} - I_{D1}^{TM}\right)\right], \tag{2e}$$

$$H_z = \frac{Il_x}{4\pi}\frac{i\sin\beta}{\omega\mu_0}\int_0^\infty \kappa^2 J_1(\kappa r) g_A^{TE}\,\mathrm{d}\kappa, \tag{2f}$$

where subscripts r and θ denote radial and tangential field components, r is the horizontal distance between the source and receiver, angle β is defined such that $\cos\beta = x/r$, Il_x is the source dipole moment with current I and dipole length l_x and subscript R denotes the layer containing the receiver. The TE- and TM-mode integrals $I_{X\{0,1\}}^{\{TE,TM\}}$ ($x \in \{A, D\}$) are given by

$$I_{X0}^{\{TE,TM\}} = \int_0^\infty \kappa J_0(\kappa r) g_X^{\{TE,TM\}}\,\mathrm{d}\kappa, \quad I_{X1}^{\{TE,TM\}} = \int_0^\infty J_1(\kappa r) g_X^{\{TE,TM\}}\,\mathrm{d}\kappa, \tag{3}$$

where $J_0(\kappa r)$ and $J_1(\kappa r)$ are the zero- and first-order Bessel functions and the integral kernels are

$$g_A^{TE} = \frac{\mu_0}{\sqrt{p_{z_R}^{TE} p_{z_S}^{TE}}}\mathcal{R}_A^{TE}, \quad g_A^{TM} = \sqrt{\frac{p_{z_R}^{TM} p_{z_S}^{TM}}{\tilde{\varepsilon}_{h_R}\tilde{\varepsilon}_{h_S}}}\mathcal{R}_A^{TM}, \tag{4a}$$

$$g_D^{TE} = -\sqrt{\frac{p_{z_R}^{TE}}{p_{z_S}^{TE}}}\mathcal{R}_D^{TE}, \quad g_D^{TM} = -\sqrt{\frac{\tilde{\varepsilon}_{h_R} p_{z_S}^{TM}}{\tilde{\varepsilon}_{h_S} p_{z_R}^{TM}}}\mathcal{R}_D^{TM}. \tag{4b}$$

The terms $\mathcal{R}_X^{\{TE,TM\}}$ describe the total response of the layered medium. For receivers located above the source ($z_R < z_S$),

$$\acute{\mathcal{R}}_X^{\{TE,TM\}} = \acute{T}_u \frac{1 + a_1\acute{R}_a}{1 - \grave{R}_u\acute{R}_a}\frac{a_2 + \grave{R}_S}{1 - \grave{R}_S\acute{R}_S}, \tag{5a}$$

where $a_1 = 1$, $a_2 = 1$ for $\acute{\mathcal{R}}_A$ and $a_1 = -1$, $a_2 = 1$ for $\acute{\mathcal{R}}_D$. For receivers located below the source ($z_R > z_S$),

$$\grave{\mathcal{R}}_X^{\{TE,TM\}} = \grave{T}_d \frac{\grave{R}_b + b_1}{1 - \acute{R}_d\grave{R}_b}\frac{1 + b_2\acute{R}_S}{1 - \acute{R}_S\grave{R}_S} \tag{5b}$$

with $b_1 = 1$, $b_2 = 1$ for $\grave{\mathcal{R}}_A$ and $b_1 = -1$, $b_2 = 1$ for $\grave{\mathcal{R}}_D$. From now, to avoid notation clutter, we will use superscripts *TE* and *TM* only where the TE- and TM-mode expressions differ and omit them otherwise.

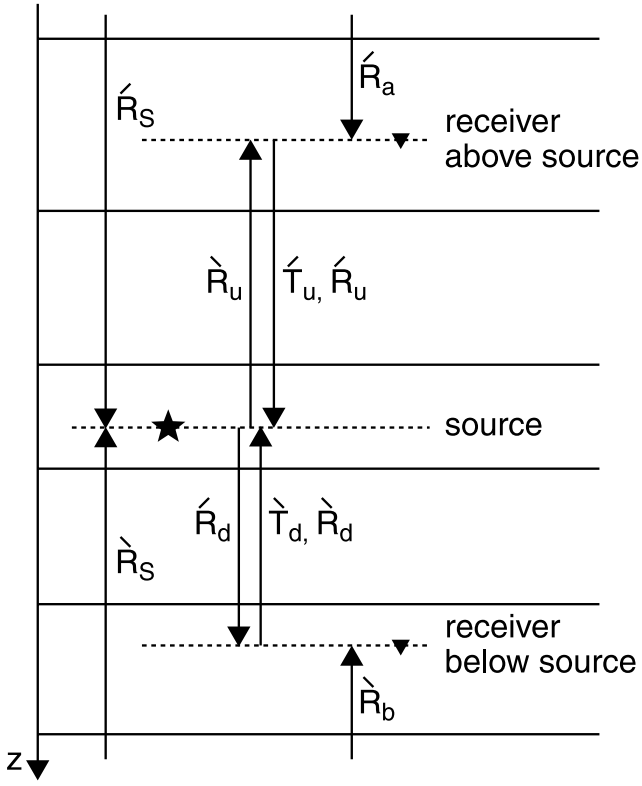

Figure 2. Layered medium reflection and transmission responses. Arrows indicate the direction of recursion.

The meaning of the separate terms in eq. (5) is illustrated in Fig. 2. $\acute{R}_S$ and $\grave{R}_S$ describe reflection responses from above and below the source. $\grave{R}_u$, $\acute{R}_d$, $\acute{T}_u$ and $\grave{T}_d$ are reflection and transmission responses from between the source and receiver, and $\acute{R}_a$ and $\grave{R}_b$ are reflection responses between the receiver and the top and bottom of the layer stack, respectively. These quantities are calculated recursively. For upward reflection and transmission, responses in layer j, just above the interface j, are given by

$$\acute{R}_j = e^{2i\omega p_{z_j} d_j} \left(\acute{r}_{j-1} + \frac{\grave{t}_{j-1} \acute{R}_{j-1} \acute{t}_{j-1}}{1 - \grave{r}_{j-1} \acute{R}_{j-1}} \right), \tag{6a}$$

$$\acute{T}_j = \frac{\acute{T}_{j-1} \acute{t}_{j-1}}{1 - \grave{r}_{j-1} \acute{R}_{j-1}} e^{i\omega p_{z_j} d_j}, \tag{6b}$$

where $\acute{r}_{j-1}$, $\grave{r}_{j-1}$, $\acute{t}_{j-1}$ and $\grave{t}_{j-1}$ are the TE or TM-mode reflection coefficients given in eq. (1). The recursion is initialized in layer 1 for $\acute{R}_S$ and $\acute{R}_a$, at the source depth for $\acute{R}_d$, and at the receiver depth for $\acute{R}_u$ and $\acute{T}_u$, with initial values $\acute{R}_{\text{ini}} = 0$, $\acute{T}_{\text{ini}} = e^{i\omega p_{z_{\text{ini}}} d_{\text{ini}}}$, where d_{ini} is the vertical distance between the receiver and the underlying layer boundary.

For downward reflection and transmission, we have in layer j, just below the interface $j - 1$,

$$\grave{R}_j = e^{2i\omega p_{z_j} d_j} \left(\grave{r}_j + \frac{\acute{t}_j \grave{R}_{j+1} \grave{t}_j}{1 - \acute{r}_j \grave{R}_{j+1}} \right), \tag{7a}$$

$$\grave{T}_j = \frac{\grave{T}_{j+1} \grave{t}_j}{1 - \acute{r}_j \grave{R}_{j+1}} e^{\mathrm{i}\omega p_{z_j} d_j}. \tag{7b}$$

The recursion is initialized in layer N for $\grave{R}_S$ and $\grave{R}_b$, at the source depth for $\grave{R}_u$, and at the receiver depth for $\grave{R}_d$ and $\grave{T}_d$, with initial values $\grave{R}_{\text{ini}} = 0$, $\grave{T}_{\text{ini}} = e^{i\omega p_{z_{\text{ini}}} d_{\text{ini}}}$ and d_{ini} being the vertical distance between the receiver and the overlying layer boundary.

3.2 Horizontal magnetic dipole source

We consider an x-directed horizontal magnetic dipole (HMD) source, that is, a small loop with area a_x, dipole moment $\mu_0 I a_x$ (Løseth & Ursin 2007), and its axis pointing in the x-direction, located at $(x, y) = (0, 0)$. The EM field components for such a source are

$$E_r = -\frac{\mathrm{i}\omega\mu_0 I a_x}{4\pi} \sin\beta \left[I_{B0}^{TM} + \frac{1}{r} \left(I_{B1}^{TE} - I_{B1}^{TM} \right) \right], \tag{8a}$$

$$E_\theta = \frac{\mathrm{i}\omega\mu_0 I a_x}{4\pi}\cos\beta\left[-I^{TE}_{B0} + \frac{1}{r}\left(I^{TE}_{B1} - I^{TM}_{B1}\right)\right], \tag{8b}$$

$$E_z = -\frac{I a_x}{4\pi}\frac{\mu_0}{\tilde{\varepsilon}_{v_R}}\sin\beta\int_0^\infty \kappa^2 J_1(\kappa r) g^{TM}_C \mathrm{d}\kappa, \tag{8c}$$

$$H_r = -\frac{\mathrm{i}\omega\mu_0 I a_x}{4\pi}\cos\beta\left[-I^{TE}_{C0} + \frac{1}{r}\left(I^{TE}_{C1} - I^{TM}_{C1}\right)\right], \tag{8d}$$

$$H_\theta = -\frac{\mathrm{i}\omega\mu_0 I a_x}{4\pi}\sin\beta\left[I^{TM}_{C0} + \frac{1}{r}\left(I^{TE}_{C1} - I^{TM}_{C1}\right)\right], \tag{8e}$$

$$H_z = \frac{I a_x}{4\pi}\cos\beta\int_0^\infty \kappa^2 J_1(\kappa r) g^{TE}_B \mathrm{d}\kappa. \tag{8f}$$

The integrals $I^{\{TE,TM\}}_{X\{0,1\}}$ ($x \in \{B, C\}$) are given by eq. (3), with

$$g^{TE}_B = \sqrt{\frac{p^{TE}_{z_S}}{p^{TE}_{z_R}}}\mathcal{R}^{TE}_B, \quad g^{TM}_B = \sqrt{\frac{p^{TM}_{z_R}\tilde{\varepsilon}_{h_S}}{\tilde{\varepsilon}_{h_R}p^{TM}_{z_S}}}\mathcal{R}^{TM}_B, \tag{9a}$$

$$g^{TE}_C = -\frac{\sqrt{p^{TE}_{z_R}p^{TE}_{z_S}}}{\mu_0}\mathcal{R}^{TE}_C, \quad g^{TM}_C = -\sqrt{\frac{\tilde{\varepsilon}_{h_R}\tilde{\varepsilon}_{h_S}}{p^{TM}_{z_R}p^{TM}_{z_S}}}\mathcal{R}^{TM}_C. \tag{9b}$$

The medium responses $\dot{\mathcal{R}}^{\{TE,TM\}}_{\{B,C\}}$ for receivers above the source are given by eq. (5a) with $a_1 = 1$, $a_2 = -1$ for $\dot{\mathcal{R}}_B$ and $a_1 = -1$, $a_2 = -1$ for $\dot{\mathcal{R}}_C$. For receivers below the source, the responses are given by eq. (5b) with $b_1 = 1$, $b_2 = -1$ for $\dot{\mathcal{R}}_B$ and $b_1 = -1$, $b_2 = -1$ for $\dot{\mathcal{R}}_C$.

3.3 Vertical electric dipole source

The EM field components for a VED source at $(x, y) = (0, 0)$ are

$$E_r = \frac{I l_z}{4\pi}\frac{\mathrm{i}}{\omega\tilde{\varepsilon}_{v_S}}\int_0^\infty \kappa^2 J_1(\kappa r) g^{TM}_B \mathrm{d}\kappa, \tag{10a}$$

$$E_z = -\frac{I l_z}{4\pi}\frac{1}{\omega^2\tilde{\varepsilon}_{v_R}\tilde{\varepsilon}_{v_S}}\int_0^\infty \kappa^3 J_0(\kappa r) g^{TM}_C \mathrm{d}\kappa + \frac{I l_z}{4\pi}\frac{1}{\mathrm{i}\omega\tilde{\varepsilon}_{v_S}}\delta(x)\delta(y)\delta(z - z_s), \tag{10b}$$

$$H_\theta = \frac{I l_z}{4\pi}\frac{\mathrm{i}}{\omega\tilde{\varepsilon}_{v_S}}\int_0^\infty \kappa^2 J_1(\kappa r) g^{TM}_C \mathrm{d}\kappa, \tag{10c}$$

where l_z is the dipole length, subscript S refers to the layer containing the source, and the TM-mode integral kernels are given in eq. (9). A VED source generates pure TM mode fields, which consist of poloidal electric (eqs 10a and b) and toroidal magnetic fields (eq. 10c); it does not generate TE fields and radial and vertical magnetic field components.

3.4 Vertical magnetic dipole source

The EM field components for a VMD source, that is, a small loop with its axis pointing in the z direction, located at $(x, y) = (0, 0)$, are

$$E_\theta = -\frac{I a_z}{4\pi}\int_0^\infty \kappa^2 J_1(\kappa r) g^{TE}_A \mathrm{d}\kappa, \tag{11a}$$

$$H_r = \frac{I a_z}{4\pi}\int_0^\infty \kappa^2 J_1(\kappa r) g^{TE}_D \mathrm{d}\kappa, \tag{11b}$$

$$H_z = \frac{I a_z}{4\pi}\frac{\mathrm{i}}{\omega\mu_0}\int_0^\infty \kappa^3 J_0(\kappa r) g^{TE}_A \mathrm{d}\kappa - \frac{I a_z}{4\pi}\delta(x)\delta(y)\delta(z - z_s). \tag{11c}$$

The TE-mode integral kernels are given in eq. (4). A VMD source generates pure TE mode fields, comprising toroidal electric (eq. 11a) and poloidal magnetic fields (eqs 11b and c); it does not generate radial and vertical electric and TM fields and does not depend on the vertical medium properties.

3.5 Long horizontal wire source

We consider a long grounded horizontal x-directed wire source centred at $(x, y) = (0, 0)$. The EM field for this source is obtained by integration over HED sources along the length of the wire. The evaluation of these integrals results in expressions in which the contributions from the

entire wire length and the grounding points can be separated (Streich & Becken 2011). Because of the integration along the x direction, it is convenient to express the EM field in terms of its Cartesian components

$$E_x = \frac{I}{4\pi}\sum_{n=1}^{N}\Delta x\int_0^\infty -\kappa g_A^{TE} J_0(\kappa r_n)\,\mathrm{d}\kappa - \frac{I}{4\pi}\sum_{n=1}^{2}(-1)^n\frac{x-x_n^S}{r_n^S}\int_0^\infty \left[g_A^{TE}-g_A^{TM}\right]J_1\left(\kappa r_n^S\right)\mathrm{d}\kappa, \tag{12a}$$

$$E_y = -\frac{I}{4\pi}\sum_{n=1}^{2}(-1)^n\frac{y}{r_n^S}\int_0^\infty \left[g_A^{TE}-g_A^{TM}\right]J_1\left(\kappa r_n^S\right)\mathrm{d}\kappa, \tag{12b}$$

$$E_z = \frac{\mathrm{i}I}{4\pi\omega\tilde{\varepsilon}_{v_R}}\sum_{n=1}^{2}(-1)^n\int_0^\infty \kappa g_D^{TM} J_0\left(\kappa r_n^S\right)\mathrm{d}\kappa, \tag{12c}$$

$$H_x = \frac{I}{4\pi}\sum_{n=1}^{2}(-1)^n\frac{y}{r_n^S}\int_0^\infty \left[g_D^{TE}-g_D^{TM}\right]J_1\left(\kappa r_n^S\right)\mathrm{d}\kappa, \tag{12d}$$

$$H_y = \frac{I}{4\pi}\sum_{n=1}^{N}\Delta x\int_0^\infty -\kappa g_D^{TE} J_0(\kappa r_n)\,\mathrm{d}\kappa - \frac{I}{4\pi}\sum_{n=1}^{2}(-1)^n\frac{x-x_n^S}{r_n^S}\int_0^\infty \left[g_D^{TE}-g_D^{TM}\right]J_1\left(\kappa r_n^S\right)\mathrm{d}\kappa, \tag{12e}$$

$$H_z = \frac{\mathrm{i}Iy}{4\pi\mu_0\omega}\sum_{n=1}^{N}\frac{\Delta x}{r_n}\int_0^\infty \kappa^2 g_A^{TE} J_1(\kappa r_n)\,\mathrm{d}\kappa. \tag{12f}$$

Here, x_n^S denotes the end points of the wire, $r_n^S = \sqrt{(x-x_n^S)^2+y^2}$, and $r_n = \sqrt{(x-x_n)^2+y^2}$ is the distance between the receiver and the n^{th} discrete wire element.

4 EM FIELD DERIVATIVES

For any field component F, we define the sensitivities $J_{F_{\{h,v\}m}}$ as the derivatives with respect to the logarithms of the horizontal and vertical conductivities of the mth layer

$$J_{F_{\{h,v\}m}} = \frac{\partial F}{\partial \ln\sigma_{\{h,v\}_m}} = \frac{\partial F}{\partial\tilde{\varepsilon}_{\{h,v\}_m}}\frac{\partial\tilde{\varepsilon}_{\{h,v\}_m}}{\partial\ln\sigma_{\{h,v\}_m}} = \frac{\partial F}{\partial\tilde{\varepsilon}_{\{h,v\}_m}}\frac{\mathrm{i}\sigma_{\{h,v\}_m}}{\omega}. \tag{13}$$

Taking derivatives with respect to $\ln\sigma$ is convenient for using the sensitivities within inversion algorithms, where $\ln\sigma$ is commonly used to bound the conductivity and ensure positive conductivity values (e.g. Constable *et al.* 1987; Newman & Alumbaugh 1997; Commer & Newman 2008). Replacing the multiplicative term $\partial\tilde{\varepsilon}_{\{h,v\}_m}/\partial\ln\sigma_{\{h,v\}_m}$ in eq. (13) by $\partial\tilde{\varepsilon}_{\{h,v\}_m}/\partial\varepsilon_{\{h,v\}_m}$ would provide sensitivities with respect to permittivity.

To facilitate recognizing analogies between the sensitivities for different field components and source types, we first present the basic building blocks contained in all derivatives, and then continue to progressively more complex blocks to finally assemble the entire derivatives of the EM field components for each source type.

4.1 Derivatives of the reflection and transmission coefficients

Derivatives of the interface reflection and transmission coefficients (eq. 1) are contained in the sensitivity expressions for all source types. Noting that all TE-mode expressions only depend on the horizontal medium properties, we find at layer boundary m

$$\frac{\partial\acute{r}_m^{TE}}{\partial\tilde{\varepsilon}_{h_m}} = \frac{-\mu_0\acute{t}_m^{TE}\grave{t}_m^{TE}}{4(p_{z_m}^{TE})^2},\quad \frac{\partial\grave{r}_m^{TE}}{\partial\tilde{\varepsilon}_{h_m}} = -\frac{\partial\acute{r}_m^{TE}}{\partial\tilde{\varepsilon}_{h_m}},$$
$$\frac{\partial\acute{t}_m^{TE}}{\partial\tilde{\varepsilon}_{h_m}} = \frac{\mu_0\acute{t}_m^{TE}\acute{r}_m^{TE}}{4(p_{z_m}^{TE})^2},\quad \frac{\partial\grave{t}_m^{TE}}{\partial\tilde{\varepsilon}_{h_m}} = \frac{\partial\acute{t}_m^{TE}}{\partial\tilde{\varepsilon}_{h_m}}, \tag{14a}$$

$$\frac{\partial\acute{r}_m^{TM}}{\partial\tilde{\varepsilon}_{h_m}} = \frac{-\acute{t}_m^{TM}\grave{t}_m^{TM}}{4\tilde{\varepsilon}_{h_m}},\quad \frac{\partial\grave{r}_m^{TM}}{\partial\tilde{\varepsilon}_{h_m}} = -\frac{\partial\acute{r}_m^{TM}}{\partial\tilde{\varepsilon}_{h_m}},$$
$$\frac{\partial\acute{t}_m^{TM}}{\partial\tilde{\varepsilon}_{h_m}} = \frac{\acute{t}_m^{TM}\acute{r}_m^{TM}}{4\tilde{\varepsilon}_{h_m}},\quad \frac{\partial\grave{t}_m^{TM}}{\partial\tilde{\varepsilon}_{h_m}} = \frac{\partial\acute{t}_m^{TM}}{\partial\tilde{\varepsilon}_{h_m}}. \tag{14b}$$

$$\frac{\partial \acute{r}_m^{TM}}{\partial \tilde{\varepsilon}_{v_m}} = \frac{p_h^2 \acute{t}_m^{TM} \grave{t}_m^{TM}}{4\tilde{\varepsilon}_{v_m}\left(\tilde{\varepsilon}_v \mu_0 - p_h^2\right)}, \quad \frac{\partial \grave{r}_m^{TM}}{\partial \tilde{\varepsilon}_{v_m}} = -\frac{\partial \acute{r}_m^{TM}}{\partial \tilde{\varepsilon}_{v_m}},$$
$$\frac{\partial \acute{t}_m^{TM}}{\partial \tilde{\varepsilon}_{v_m}} = \frac{-p_h^2 \acute{t}_m^{TM} \acute{r}_m^{TM}}{4\tilde{\varepsilon}_{v_m}\left(\tilde{\varepsilon}_v \mu_0 - p_h^2\right)}, \quad \frac{\partial \grave{t}_m^{TM}}{\partial \tilde{\varepsilon}_{v_m}} = \frac{\partial \acute{t}_m^{TM}}{\partial \tilde{\varepsilon}_{v_m}}. \tag{14c}$$

Because the properties of the mth layer are also contained in the reflection and transmission coefficients for layer boundary $m-1$, we also require

$$\frac{\partial \acute{r}_{m-1}^{TE}}{\partial \tilde{\varepsilon}_{h_m}} = \frac{\mu_0 \acute{t}_{m-1}^{TE} \grave{t}_{m-1}^{TE}}{4(p_{z_m}^{TE})^2}, \quad \frac{\partial \grave{r}_{m-1}^{TE}}{\partial \tilde{\varepsilon}_{h_m}} = -\frac{\partial \acute{r}_{m-1}^{TE}}{\partial \tilde{\varepsilon}_{h_m}},$$
$$\frac{\partial \acute{t}_{m-1}^{TE}}{\partial \tilde{\varepsilon}_{h_m}} = -\frac{\mu_0 \acute{t}_{m-1}^{TE} \acute{r}_{m-1}^{TE}}{4(p_{z_m}^{TE})^2}, \quad \frac{\partial \grave{t}_{m-1}^{TE}}{\partial \tilde{\varepsilon}_{h_m}} = \frac{\partial \acute{t}_{m-1}^{TE}}{\partial \tilde{\varepsilon}_{h_m}}, \tag{15a}$$

$$\frac{\partial \acute{r}_{m-1}^{TM}}{\partial \tilde{\varepsilon}_{h_m}} = \frac{\acute{t}_{m-1}^{TM} \grave{t}_{m-1}^{TM}}{4\tilde{\varepsilon}_{h_m}}, \quad \frac{\partial \grave{r}_{m-1}^{TM}}{\partial \tilde{\varepsilon}_{h_m}} = -\frac{\partial \acute{r}_{m-1}^{TM}}{\partial \tilde{\varepsilon}_{h_m}},$$
$$\frac{\partial \acute{t}_{m-1}^{TM}}{\partial \tilde{\varepsilon}_{h_m}} = -\frac{\acute{t}_{m-1}^{TM} \acute{r}_{m-1}^{TM}}{4\tilde{\varepsilon}_{h_m}}, \quad \frac{\partial \grave{t}_{m-1}^{TM}}{\partial \tilde{\varepsilon}_{h_m}} = \frac{\partial \acute{t}_{m-1}^{TM}}{\partial \tilde{\varepsilon}_{h_m}}. \tag{15b}$$

$$\frac{\partial \acute{r}_{m-1}^{TM}}{\partial \tilde{\varepsilon}_{v_m}} = \frac{-p_h^2 \acute{t}_{m-1}^{TM} \grave{t}_{m-1}^{TM}}{4\tilde{\varepsilon}_{v_m}\left(\tilde{\varepsilon}_{v_m} \mu_0 - p_h^2\right)}, \quad \frac{\partial \grave{r}_{m-1}^{TM}}{\partial \tilde{\varepsilon}_{v_m}} = -\frac{\partial \acute{r}_{m-1}^{TM}}{\partial \tilde{\varepsilon}_{v_m}},$$
$$\frac{\partial \acute{t}_{m-1}^{TM}}{\partial \tilde{\varepsilon}_{v_m}} = \frac{p_h^2 \acute{t}_{m-1}^{TM} \acute{r}_{m-1}^{TM}}{4\tilde{\varepsilon}_{v_m}\left(\tilde{\varepsilon}_{v_m} \mu_0 - p_h^2\right)}, \quad \frac{\partial \grave{t}_{m-1}^{TM}}{\partial \tilde{\varepsilon}_{v_m}} = \frac{\partial \acute{t}_{m-1}^{TM}}{\partial \tilde{\varepsilon}_{v_m}}. \tag{15c}$$

4.2 Derivatives of the recursive reflection and transmission responses

4.2.1 Upward reflection

The next building blocks contained in the sensitivities for all source types are the derivatives of the recursive reflection and transmission responses given in eqs (6) and (7). We first consider upward reflection (i.e. the derivatives $\partial \acute{R}/\partial \tilde{\varepsilon}_{h_m}$ and $\partial \acute{R}/\partial \tilde{\varepsilon}_{v_m}$ with respect to the mth layer). The reflection responses $\acute{R}$ contain the properties of all layers above the source for $\acute{R}_S$, above the receiver for $\acute{R}_a$, and between the source and receiver for $\acute{R}_d$ (Fig. 2), resulting in non-zero derivatives only if layer m is one of these layers. In the initial layer, we have $\acute{R}_{\text{ini}} = 0$ and hence also $\partial \acute{R}_{\text{ini}}/\partial \tilde{\varepsilon}_m = 0$. Also, $\partial \acute{R}_k/\partial \tilde{\varepsilon}_m = 0$ for $k < m$ (i.e. everywhere above layer m). As the recursion proceeds to layer m, we use the chain rule of differentiation to obtain

$$\frac{\partial \acute{R}_m}{\partial \tilde{\varepsilon}_m} = \frac{\partial \acute{R}_m}{\partial E_m^2}\frac{\partial E_m^2}{\partial \tilde{\varepsilon}_m} + \frac{\partial \acute{R}_m}{\partial \acute{r}_{m-1}}\frac{\partial \acute{r}_{m-1}}{\partial \tilde{\varepsilon}_m} + 2\frac{\partial \acute{R}_m}{\partial \grave{t}_{m-1}}\frac{\partial \grave{t}_{m-1}}{\partial \tilde{\varepsilon}_m} + \frac{\partial \acute{R}_m}{\partial \grave{r}_{m-1}}\frac{\partial \grave{r}_{m-1}}{\partial \tilde{\varepsilon}_m}. \tag{16}$$

Here, $E_m = e^{\mathrm{i}\omega p_{z_m} d_m}$ and we have used $\acute{t}_{m-1} = \grave{t}_{m-1}$. The TE and TM-mode derivatives of the interface reflection and transmission coefficients are given in eq. (15). Evaluating the remaining terms of eq. (16) results in

$$\frac{\partial \acute{R}_m}{\partial E_m^2} = \acute{r}_{m-1} + \frac{\grave{t}_{m-1}\acute{R}_{m-1}\acute{t}_{m-1}}{1 - \grave{r}_{m-1}\acute{R}_{m-1}}, \tag{17a}$$

$$\frac{\partial \acute{R}_m}{\partial \acute{r}_{m-1}} = E_m^2, \tag{17b}$$

$$\frac{\partial \acute{R}_m}{\partial \grave{t}_{m-1}} = E_m^2 \frac{\acute{R}_{m-1}\acute{t}_{m-1}}{1 - \grave{r}_{m-1}\acute{R}_{m-1}}, \tag{17c}$$

$$\frac{\partial \acute{R}_m}{\partial \grave{r}_{m-1}} = E_m^2 \frac{\grave{t}_{m-1}\acute{R}_{m-1}^2\acute{t}_{m-1}}{(1 - \grave{r}_{m-1}\acute{R}_{m-1})^2}, \tag{17d}$$

$$\frac{\partial E_m^{TE^2}}{\partial \tilde{\varepsilon}_{h_m}} = \frac{\mathrm{i}\omega\mu_0 d_m}{p_{z_m}^{TE}} e^{2\mathrm{i}\omega p_{z_m}^{TE} d_m}, \tag{17e}$$

$$\frac{\partial E_m^{TM^2}}{\partial \tilde{\varepsilon}_{h_m}} = \frac{\mathrm{i}\omega d_m \left(\mu_0 - \frac{p_h^2}{\tilde{\varepsilon}_{v_m}}\right)}{p_{z_m}^{TM}} e^{2\mathrm{i}\omega p_{z_m}^{TM} d_m}, \tag{17f}$$

$$\frac{\partial E_m^{TM^2}}{\partial \tilde{\varepsilon}_{v_m}} = \frac{\mathrm{i}\omega d_m \tilde{\varepsilon}_{h_m} p_h^2}{\tilde{\varepsilon}_{v_m}^2 p_{z_m}^{TM}} e^{2\mathrm{i}\omega p_{z_m}^{TM} d_m}. \tag{17g}$$

Eq. (16) then becomes

$$\frac{\partial \acute{R}_m}{\partial \tilde{\varepsilon}_m} = C_1 \acute{R}_m + E_m^2 C_2 \acute{t}_{m-1}^2 \left[1 - \frac{2\acute{R}_{m-1}\acute{r}_{m-1}}{1 - \grave{r}_{m-1}\acute{R}_{m-1}} - \frac{\grave{t}_{m-1}^2 \acute{R}_{m-1}^2}{(1 - \grave{r}_{m-1}\acute{R}_{m-1})^2} \right]. \tag{18}$$

The factors C_1 and C_2 are for $\partial \acute{R}_m^{TE}/\partial \tilde{\varepsilon}_{h_m}$

$$C_1 = \frac{\mathrm{i}\omega\mu_0 d_m}{p_{z_m}^{TE}}, \quad C_2 = \frac{\mu_0}{4(p_{z_m}^{TE})^2}, \tag{19a}$$

for $\partial \acute{R}_m^{TM}/\partial \tilde{\varepsilon}_{h_m}$

$$C_1 = \frac{\mathrm{i}\omega d_m \left(\mu_0 - \frac{p_h^2}{\tilde{\varepsilon}_{v_m}}\right)}{p_{z_m}^{TM}}, \quad C_2 = \frac{1}{4\tilde{\varepsilon}_{h_m}}, \tag{19b}$$

and for $\partial \acute{R}_m^{TM}/\partial \tilde{\varepsilon}_{v_m}$

$$C_1 = \frac{\mathrm{i}\omega d_m \tilde{\varepsilon}_{h_m} p_h^2}{\tilde{\varepsilon}_{v_m}^2 p_{z_m}^{TM}}, \quad C_2 = -\frac{p_h^2}{4\tilde{\varepsilon}_{v_m}\left(\tilde{\varepsilon}_{v_m}\mu_0 - p_h^2\right)}. \tag{19c}$$

If the recursion proceeds to layer $m+1$, we have to consider the derivative $\partial \acute{R}_{m+1}/\partial \tilde{\varepsilon}_m$. Here, the properties $\tilde{\varepsilon}_m$ of layer m are not contained in the exponential term $e^{\mathrm{i}\omega p_{z_{m+1}} d_{m+1}}$. Instead, we now have to consider the partial derivatives with respect to $\acute{R}_m$

$$\frac{\partial \acute{R}_{m+1}}{\partial \tilde{\varepsilon}_m} = \frac{\partial \acute{R}_{m+1}}{\partial \acute{r}_m}\frac{\partial \acute{r}_m}{\partial \tilde{\varepsilon}_m} + 2\frac{\partial \acute{R}_{m+1}}{\partial \grave{t}_m}\frac{\partial \grave{t}_m}{\partial \tilde{\varepsilon}_m} + \frac{\partial \acute{R}_{m+1}}{\partial \grave{r}_m}\frac{\partial \grave{r}_m}{\partial \tilde{\varepsilon}_m} + \frac{\partial \acute{R}_{m+1}}{\partial \acute{R}_m}\frac{\partial \acute{R}_m}{\partial \tilde{\varepsilon}_m}. \tag{20}$$

We find

$$\frac{\partial \acute{R}_{m+1}}{\partial \acute{R}_m} = E_{m+1}^2 \frac{\grave{t}_m \acute{t}_m}{(1 - \grave{r}_m \acute{R}_m)^2}, \tag{21}$$

and all other partial derivatives are given in eqs (14), (17) (with $m \to m+1$) and (18). Assembling all terms, we obtain

$$\frac{\partial \acute{R}_{m+1}}{\partial \tilde{\varepsilon}_m} = -E_{m+1}^2 C_2 \acute{t}_m^2 \left[1 - \frac{2\acute{R}_m \acute{r}_m}{1 - \grave{r}_m \acute{R}_m} - \frac{\grave{t}_m^2 \acute{R}_m^2}{(1 - \grave{r}_m \acute{R}_m)^2} \right] + \frac{E_{m+1}^2 \acute{t}_m^2}{(1 - \grave{r}_m \acute{R}_m)^2}\frac{\partial \acute{R}_m}{\partial \tilde{\varepsilon}_m}, \tag{22}$$

where C_2 for the different derivatives $\partial \acute{R}_{m+1}^{TE}/\partial \tilde{\varepsilon}_{h_m}$, $\partial \acute{R}_{m+1}^{TM}/\partial \tilde{\varepsilon}_{h_m}$ and $\partial \acute{R}_{m+1}^{TM}/\partial \tilde{\varepsilon}_{v_m}$ is given by eq. (19a, b and c), respectively.

For layers $k \geq m+2$, the interface reflection and transmission coefficients do not depend on $\tilde{\varepsilon}_m$. Therefore, we obtain the recursive expression

$$\frac{\partial \acute{R}_k}{\partial \tilde{\varepsilon}_m} = \frac{\partial \acute{R}_k}{\partial \acute{R}_{k-1}}\frac{\partial \acute{R}_{k-1}}{\partial \tilde{\varepsilon}_m} = \frac{E_k^2 \acute{t}_{k-1}^2}{(1 - \grave{r}_{k-1}\acute{R}_{k-1})^2}\frac{\partial \acute{R}_{k-1}}{\partial \tilde{\varepsilon}_m}; \quad k \geq m+2. \tag{23}$$

4.2.2 Upward transmission

For the upward transmission response, differentiation gives for layer m

$$\frac{\partial \acute{T}_m}{\partial \tilde{\varepsilon}_m} = \frac{\partial \acute{T}_m}{\partial \acute{t}_{m-1}}\frac{\partial \acute{t}_{m-1}}{\partial \tilde{\varepsilon}_m} + \frac{\partial \acute{T}_m}{\partial \grave{r}_{m-1}}\frac{\partial \grave{r}_{m-1}}{\partial \tilde{\varepsilon}_m} + \frac{\partial \acute{T}_m}{\partial E_m}\frac{\partial E_m}{\partial \tilde{\varepsilon}_m}. \tag{24}$$

Using eq. (15) and

$$\frac{\partial \acute{T}_m}{\partial \acute{t}_{m-1}} = E_m \frac{\acute{T}_{m-1}}{1 - \grave{r}_{m-1}\acute{R}_{m-1}}, \tag{25a}$$

$$\frac{\partial \acute{T}_m}{\partial \grave{r}_{m-1}} = E_m \frac{\acute{T}_{m-1}\acute{t}_{m-1}\acute{R}_{m-1}}{(1 - \grave{r}_{m-1}\acute{R}_{m-1})^2}, \tag{25b}$$

$$\frac{\partial \acute{T}_m}{\partial E_m} = \frac{\acute{T}_{m-1}\acute{t}_{m-1}}{1 - \grave{r}_{m-1}\acute{R}_{m-1}}, \tag{25c}$$

$$\frac{\partial E_m^{TE}}{\partial \tilde{\varepsilon}_{h_m}} = \frac{\mathrm{i}\omega\mu_0 d_m}{2p_{z_m}^{TE}} E_m, \tag{25d}$$

$$\frac{\partial E_m^{TM}}{\partial \tilde{\varepsilon}_{h_m}} = \frac{\mathrm{i}\omega d_m \left(\mu_0 - \frac{p_h^2}{\tilde{\varepsilon}_{v_m}}\right)}{2p_{z_m}^{TM}} e^{2\mathrm{i}\omega p_{z_m}^{TM} d_m}, \tag{25e}$$

$$\frac{\partial E_m^{TM}}{\partial \tilde{\varepsilon}_{v_m}} = \frac{\mathrm{i}\omega d_m \tilde{\varepsilon}_{h_m} p_h^2}{2\tilde{\varepsilon}_{v_m}^2 p_{z_m}^{TM}} e^{2\mathrm{i}\omega p_{z_m}^{TM} d_m}. \tag{25f}$$

we obtain

$$\frac{\partial \acute{T}_m}{\partial \tilde{\varepsilon}_m} = \frac{C_1}{2}\acute{T}_m - \frac{E_m C_2 \acute{T}_{m-1}\acute{t}_{m-1}}{(1-\grave{r}_{m-1}\acute{R}_{m-1})}\left[\acute{r}_{m-1} + \frac{\acute{R}_{m-1}\acute{t}^2_{m-1}}{(1-\grave{r}_{m-1}\acute{R}_{m-1})}\right], \tag{26}$$

where C_1 and C_2 are given by eq. (19).

For layer $m+1$, the exponential term no longer depends on $\tilde{\varepsilon}_m$, but we now have to consider the dependency of $\acute{T}_m$ and $\acute{R}_m$ on $\tilde{\varepsilon}_m$. Accordingly,

$$\frac{\partial \acute{T}_{m+1}}{\partial \tilde{\varepsilon}_m} = \frac{\partial \acute{T}_{m+1}}{\partial \acute{t}_m}\frac{\partial \acute{t}_m}{\partial \tilde{\varepsilon}_m} + \frac{\partial \acute{T}_{m+1}}{\partial \grave{r}_m}\frac{\partial \grave{r}_m}{\partial \tilde{\varepsilon}_m} + \frac{\partial \acute{T}_{m+1}}{\partial \acute{T}_m}\frac{\partial \acute{T}_m}{\partial \tilde{\varepsilon}_m} + \frac{\partial \acute{T}_{m+1}}{\partial \acute{R}_m}\frac{\partial \acute{R}_m}{\partial \tilde{\varepsilon}_m}. \tag{27}$$

Using eqs (14), (25) (with $m \rightarrow m+1$), (18), (26) and

$$\frac{\partial \acute{T}_{m+1}}{\partial \acute{T}_m} = E_{m+1}\frac{\acute{t}_m}{1-\grave{r}_m\acute{R}_m}, \tag{28a}$$

$$\frac{\partial \acute{T}_{m+1}}{\partial \acute{R}_m} = E_{m+1}\frac{\acute{T}_m\acute{t}_m\grave{r}_m}{(1-\grave{r}_m\acute{R}_m)^2}, \tag{28b}$$

the three different expressions for the derivatives of the transmission responses are obtained as

$$\frac{\partial \acute{T}_{m+1}}{\partial \tilde{\varepsilon}_m} = \frac{E_{m+1}C_2\acute{T}_m\acute{t}_m}{(1-\grave{r}_m\acute{R}_m)}\left[\acute{r}_m + \frac{\acute{R}_m\acute{t}^2_m}{(1-\grave{r}_m\acute{R}_m)}\right] + \frac{E_{m+1}\acute{t}_m}{(1-\grave{r}_m\acute{R}_m)}\left[\frac{\partial \acute{T}_m}{\partial \tilde{\varepsilon}_m} + \frac{\acute{T}_m\grave{r}_m}{(1-\grave{r}_m\acute{R}_m)}\frac{\partial \acute{R}_m}{\partial \tilde{\varepsilon}_m}\right]. \tag{29}$$

For subsequent layers $k \geq m+2$, where the interface reflection and transmission coefficients are independent of $\tilde{\varepsilon}_m$, we obtain

$$\frac{\partial \acute{T}_k}{\partial \tilde{\varepsilon}_m} = \frac{E_k\acute{t}_{k-1}}{(1-\grave{r}_{k-1}\acute{R}_{k-1})}\left[\frac{\partial \acute{T}_{k-1}}{\partial \tilde{\varepsilon}_m} + \frac{\acute{T}_{k-1}\grave{r}_{k-1}}{(1-\grave{r}_{k-1}\acute{R}_{k-1})}\frac{\partial \acute{R}_{k-1}}{\partial \tilde{\varepsilon}_m}\right]. \tag{30}$$

4.2.3 Downward reflection and transmission

Using analogous derivations as shown in Section 4.2.1, we find the derivatives of the downward reflection responses (eq. 7a) for layer m

$$\frac{\partial \grave{R}_m}{\partial \tilde{\varepsilon}_m} = C_1\grave{R}_m + E_m^2 C_2 \acute{t}_m^2\left[1 - \frac{2\grave{R}_{m+1}\grave{r}_m}{1-\acute{r}_m\grave{R}_{m+1}} - \frac{\acute{t}_m^2\grave{R}^2_{m+1}}{(1-\acute{r}_m\grave{R}_{m+1})^2}\right], \tag{31}$$

for layer $m-1$,

$$\frac{\partial \grave{R}_{m-1}}{\partial \tilde{\varepsilon}_m} = -E^2_{m-1}C_2\acute{t}^2_{m-1}\left[1 - \frac{2\grave{R}_m\grave{r}_{m-1}}{1-\acute{r}_{m-1}\grave{R}_m} - \frac{\acute{t}^2_{m-1}\grave{R}^2_m}{(1-\acute{r}_{m-1}\grave{R}_m)^2}\right] + \frac{E^2_{m-1}\acute{t}^2_{m-1}}{(1-\acute{r}_{m-1}\grave{R}_m)^2}\frac{\partial \grave{R}_m}{\partial \tilde{\varepsilon}_m}, \tag{32}$$

and for further layers $k \leq m-2$,

$$\frac{\partial \grave{R}_k}{\partial \tilde{\varepsilon}_m} = \frac{\partial \grave{R}_k}{\partial \grave{R}_{k+1}}\frac{\partial \grave{R}_{k+1}}{\partial \tilde{\varepsilon}_m} = \frac{E_k^2\acute{t}_k^2}{(1-\acute{r}_k\grave{R}_{k+1})^2}\frac{\partial \grave{R}_{k+1}}{\partial \tilde{\varepsilon}_m}. \tag{33}$$

Analogously to the derivations in Section 4.2.2, derivatives of the downward transmission responses (eq. 7b) are for layer m

$$\frac{\partial \grave{T}_m}{\partial \tilde{\varepsilon}_m} = \frac{C_1}{2}\grave{T}_m - \frac{E_m C_2 \grave{T}_{m+1}\acute{t}_m}{(1-\acute{r}_m\grave{R}_{m+1})}\left[\grave{r}_m + \frac{\grave{R}_{m+1}\acute{t}^2_m}{(1-\acute{r}_m\grave{R}_{m+1})}\right], \tag{34}$$

for layer $m-1$,

$$\frac{\partial \grave{T}_{m-1}}{\partial \tilde{\varepsilon}_m} = \frac{E_{m-1}C_2\grave{T}_m\acute{t}_{m-1}}{(1-\acute{r}_{m-1}\grave{R}_m)}\left[\grave{r}_{m-1} + \frac{\grave{R}_m\acute{t}^2_{m-1}}{(1-\acute{r}_{m-1}\grave{R}_m)}\right] + \frac{E_{m-1}\grave{t}_{m-1}}{(1-\acute{r}_{m-1}\grave{R}_m)}\left[\frac{\partial \grave{T}_m}{\partial \tilde{\varepsilon}_m} + \frac{\grave{T}_m\acute{r}_{m-1}}{(1-\acute{r}_{m-1}\grave{R}_m)}\frac{\partial \grave{R}_m}{\partial \tilde{\varepsilon}_m}\right], \tag{35}$$

and for further layers $k \leq m-2$,

$$\frac{\partial \grave{T}_k}{\partial \tilde{\varepsilon}_m} = \frac{E_k\grave{t}_k}{(1-\acute{r}_k\grave{R}_{k+1})}\left[\frac{\partial \grave{T}_{k+1}}{\partial \tilde{\varepsilon}_m} + \frac{\grave{T}_{k+1}\acute{r}_k}{(1-\acute{r}_k\grave{R}_{k+1})}\frac{\partial \grave{R}_{k+1}}{\partial \tilde{\varepsilon}_m}\right]. \tag{36}$$

4.3 Derivatives of the total reflection and transmission responses

We now take the derivatives of the total medium responses that describe all EM field propagation between the source and receiver depths, that is, the derivatives of eq. (5). For receivers located above the source ($z_R < z_S$),

$$\frac{\partial \acute{\mathcal{R}}_X}{\partial \tilde{\varepsilon}_m} = \frac{\partial \acute{\mathcal{R}}_X}{\partial \acute{T}_u}\frac{\partial \acute{T}_u}{\partial \tilde{\varepsilon}_m} + \frac{\partial \acute{\mathcal{R}}_X}{\partial \acute{R}_a}\frac{\partial \acute{R}_a}{\partial \tilde{\varepsilon}_m} + \frac{\partial \acute{\mathcal{R}}_X}{\partial \grave{R}_u}\frac{\partial \grave{R}_u}{\partial \tilde{\varepsilon}_m} + \frac{\partial \acute{\mathcal{R}}_X}{\partial \grave{R}_S}\frac{\partial \grave{R}_S}{\partial \tilde{\varepsilon}_m} + \frac{\partial \acute{\mathcal{R}}_X}{\partial \acute{R}_S}\frac{\partial \acute{R}_S}{\partial \tilde{\varepsilon}_m}, \tag{37}$$

$$\frac{\partial \acute{\mathcal{R}}_X}{\partial \acute{T}_u} = \frac{1 + a_1 \acute{R}_a}{1 - \grave{R}_u \acute{R}_a}\frac{a_2 + \grave{R}_S}{1 - \grave{R}_S \acute{R}_S}, \tag{38a}$$

$$\frac{\partial \acute{\mathcal{R}}_X}{\partial \acute{R}_a} = \acute{T}_u \frac{\grave{R}_u + a_1}{(1 - \grave{R}_u \acute{R}_a)^2}\frac{\grave{R}_S + a_2}{1 - \grave{R}_S \acute{R}_S}, \tag{38b}$$

$$\frac{\partial \acute{\mathcal{R}}_X}{\partial \grave{R}_u} = \acute{T}_u \frac{(1 + a_1 \acute{R}_a)\acute{R}_a}{(1 - \grave{R}_u \acute{R}_a)^2}\frac{\grave{R}_S + a_2}{1 - \grave{R}_S \acute{R}_S}, \tag{38c}$$

$$\frac{\partial \acute{\mathcal{R}}_X}{\partial \grave{R}_S} = \acute{T}_u \frac{1 + a_1 \acute{R}_a}{1 - \grave{R}_u \acute{R}_a}\frac{1 + a_2 \acute{R}_S}{(1 - \grave{R}_S \acute{R}_S)^2}, \tag{38d}$$

$$\frac{\partial \acute{\mathcal{R}}_X}{\partial \acute{R}_S} = \acute{T}_u \frac{1 + a_1 \acute{R}_a}{1 - \grave{R}_u \acute{R}_a}\frac{(\grave{R}_S + a_2)\grave{R}_S}{(1 - \grave{R}_S \acute{R}_S)^2}, \tag{38e}$$

with $X \in \{A, B, C, D\}$ and $a_1 = 1, a_2 = 1$ for $\acute{\mathcal{R}}_A$, $a_1 = 1, a_2 = -1$ for $\acute{\mathcal{R}}_B$, $a_1 = -1, a_2 = -1$ for $\acute{\mathcal{R}}_C$ and $a_1 = -1, a_2 = 1$ for $\acute{\mathcal{R}}_D$. Recursive expressions describing the partial derivatives with respect to $\tilde{\varepsilon}_m$ are given by eqs (18), (22) and (23) for $\acute{R}_S$ and $\acute{R}_a$, eqs (31), (32) and (33) for $\grave{R}_S$ and $\grave{R}_u$, and eqs (26), (29) and (30) for $\acute{T}_u$.

For receivers below the source ($z_R > z_S$), the derivative of the total reflection response is given by

$$\frac{\partial \grave{\mathcal{R}}_X}{\partial \tilde{\varepsilon}_m} = \frac{\partial \grave{\mathcal{R}}_X}{\partial \grave{T}_d}\frac{\partial \grave{T}_d}{\partial \tilde{\varepsilon}_m} + \frac{\partial \grave{\mathcal{R}}_X}{\partial \grave{R}_b}\frac{\partial \grave{R}_b}{\partial \tilde{\varepsilon}_m} + \frac{\partial \grave{\mathcal{R}}_X}{\partial \acute{R}_d}\frac{\partial \acute{R}_d}{\partial \tilde{\varepsilon}_m} + \frac{\partial \grave{\mathcal{R}}_X}{\partial \acute{R}_S}\frac{\partial \acute{R}_S}{\partial \tilde{\varepsilon}_m} + \frac{\partial \grave{\mathcal{R}}_X}{\partial \grave{R}_S}\frac{\partial \grave{R}_S}{\partial \tilde{\varepsilon}_m}, \tag{39}$$

$$\frac{\partial \grave{\mathcal{R}}_X}{\partial \grave{T}_d} = \frac{\grave{R}_b + b_1}{1 - \acute{R}_d \grave{R}_b}\frac{1 + b_2 \acute{R}_S}{1 - \acute{R}_S \grave{R}_S}, \tag{40a}$$

$$\frac{\partial \grave{\mathcal{R}}_X}{\partial \grave{R}_b} = \grave{T}_d \frac{1 + b_1 \acute{R}_d}{(1 - \acute{R}_d \grave{R}_b)^2}\frac{1 + b_2 \acute{R}_S}{1 - \acute{R}_S \grave{R}_S}, \tag{40b}$$

$$\frac{\partial \grave{\mathcal{R}}_X}{\partial \acute{R}_d} = \grave{T}_d \frac{(\grave{R}_b + b_1)\grave{R}_b}{(1 - \acute{R}_d \grave{R}_b)^2}\frac{1 + b_2 \acute{R}_S}{1 - \acute{R}_S \grave{R}_S}, \tag{40c}$$

$$\frac{\partial \grave{\mathcal{R}}_X}{\partial \acute{R}_S} = \grave{T}_d \frac{\grave{R}_b + b_1}{1 - \acute{R}_d \grave{R}_b}\frac{\grave{R}_S + b_2}{(1 - \acute{R}_S \grave{R}_S)^2}, \tag{40d}$$

$$\frac{\partial \grave{\mathcal{R}}_X}{\partial \grave{R}_S} = \grave{T}_d \frac{\grave{R}_b + b_1}{1 - \acute{R}_d \grave{R}_b}\frac{(1 + b_2 \acute{R}_S)\acute{R}_S}{(1 - \acute{R}_S \grave{R}_S)^2}, \tag{40e}$$

with $b_1 = 1, b_2 = 1$ for $\grave{\mathcal{R}}_A$, $b_1 = 1, b_2 = -1$ for $\grave{\mathcal{R}}_B$, $b_1 = -1, b_2 = -1$ for $\grave{\mathcal{R}}_C$ and $b_1 = -1, b_2 = 1$ for $\grave{\mathcal{R}}_D$. Recursive expressions describing the partial derivatives with respect to $\tilde{\varepsilon}_m$ are given by eqs (18), (22) and (23) for $\acute{R}_S$ and $\acute{R}_d$, eqs (31), (32) and (33) for $\grave{R}_S$ and $\grave{R}_b$, and eqs (34), (35) and (36) for $\grave{T}_d$.

4.4 Derivatives of the integral kernels

We now evaluate the derivatives of the integral kernels given in eqs (4) and (9). For $z_R < z_S$, each expression $\partial g_X^{TE}/\partial \tilde{\varepsilon}_{h_m}$ and $\partial g_X^{TM}/\partial \tilde{\varepsilon}_{\{h,v\}_m}$ contains the derivatives of the medium reflection responses from eqs (37) and (38). For $z_R > z_S$, the kernels $\partial g_X^{TE}/\partial \tilde{\varepsilon}_{h_m}$ and $\partial g_X^{TM}/\partial \tilde{\varepsilon}_{\{h,v\}_m}$ contain the expressions from eqs (39) and (40). Then,

$$\begin{aligned}\frac{\partial g_A^{TE}}{\partial \tilde{\varepsilon}_{h_m}} &= \frac{\partial g_A^{TE}}{\partial p_{z_R}^{TE}}\frac{\partial p_{z_R}^{TE}}{\partial \tilde{\varepsilon}_{h_m}} + \frac{\partial g_A^{TE}}{\partial p_{z_S}^{TE}}\frac{\partial p_{z_S}^{TE}}{\partial \tilde{\varepsilon}_{h_m}} + \frac{\partial g_A^{TE}}{\partial \mathcal{R}_A^{TE}}\frac{\partial \mathcal{R}_A^{TE}}{\partial \tilde{\varepsilon}_{h_m}} \\ &= \frac{\mu_0}{\sqrt{p_{z_R}^{TE} p_{z_S}^{TE}}}\left(-(\delta_{Rm} + \delta_{Sm})\frac{\mu_0}{4 p_{z_m}^{TE^2}}\mathcal{R}_A^{TE} + \frac{\partial \mathcal{R}_A^{TE}}{\partial \tilde{\varepsilon}_{h_m}}\right),\end{aligned} \tag{41a}$$

where δ_{Rm} and δ_{Sm} are =1 if the receiver/source is located in layer m, and =0 otherwise, and $\partial \mathcal{R}_A^{TE}/\partial \tilde{\varepsilon}_{h_m}$ is given either by eq (37) or (39). Similarly,

$$\frac{\partial g_A^{TM}}{\partial \tilde{\varepsilon}_{h_m}} = \sqrt{\frac{p_{z_R}^{TM} p_{z_S}^{TM}}{\tilde{\varepsilon}_{h_R} \tilde{\varepsilon}_{h_S}}} \left(-\frac{(\delta_{Rm} + \delta_{Sm})}{2} \left(\frac{1}{\tilde{\varepsilon}_{h_m}} - \frac{\mu_0 - \frac{p_h^2}{\tilde{\varepsilon}_{v_m}}}{2 p_{z_m}^{TM^2}} \right) \mathcal{R}_A^{TM} + \frac{\partial \mathcal{R}_A^{TM}}{\partial \tilde{\varepsilon}_{h_m}} \right), \tag{41b}$$

$$\frac{\partial g_A^{TM}}{\partial \tilde{\varepsilon}_{v_m}} = \sqrt{\frac{p_{z_R}^{TM} p_{z_S}^{TM}}{\tilde{\varepsilon}_{h_R} \tilde{\varepsilon}_{h_S}}} \left((\delta_{Rm} + \delta_{Sm}) \frac{\tilde{\varepsilon}_{h_m} p_h^2}{4 \tilde{\varepsilon}_{v_m}^2 p_{z_m}^{TM^2}} \mathcal{R}_A^{TM} + \frac{\partial \mathcal{R}_A^{TM}}{\partial \tilde{\varepsilon}_{v_m}} \right), \tag{41c}$$

$$\frac{\partial g_D^{TE}}{\partial \tilde{\varepsilon}_{h_m}} = -\sqrt{\frac{p_{z_R}^{TE}}{p_{z_S}^{TE}}} \left((\delta_{Rm} - \delta_{Sm}) \frac{\mu_0}{4 p_{z_m}^{TE^2}} \mathcal{R}_D^{TE} + \frac{\partial \mathcal{R}_D^{TE}}{\partial \tilde{\varepsilon}_{h_m}} \right), \tag{42a}$$

$$\frac{\partial g_D^{TM}}{\partial \tilde{\varepsilon}_{h_m}} = -\sqrt{\frac{\tilde{\varepsilon}_{h_R} p_{z_S}^{TM}}{\tilde{\varepsilon}_{h_S} p_{z_R}^{TM}}} \left(\frac{(\delta_{Rm} - \delta_{Sm})}{2} \left(\frac{1}{\tilde{\varepsilon}_{h_m}} - \frac{\mu_0 - \frac{p_h^2}{\tilde{\varepsilon}_{v_m}}}{2 p_{z_m}^{TM^2}} \right) \mathcal{R}_D^{TM} + \frac{\partial \mathcal{R}_D^{TM}}{\partial \tilde{\varepsilon}_{h_m}} \right), \tag{42b}$$

$$\frac{\partial g_D^{TM}}{\partial \tilde{\varepsilon}_{v_m}} = -\sqrt{\frac{\tilde{\varepsilon}_{h_R} p_{z_S}^{TM}}{\tilde{\varepsilon}_{h_S} p_{z_R}^{TM}}} \left(-(\delta_{Rm} - \delta_{Sm}) \frac{\tilde{\varepsilon}_{h_m} p_h^2}{4 \tilde{\varepsilon}_{v_m}^2 p_{z_m}^{TM^2}} \mathcal{R}_D^{TM} + \frac{\partial \mathcal{R}_D^{TM}}{\partial \tilde{\varepsilon}_{v_m}} \right), \tag{42c}$$

$$\frac{\partial g_B^{TE}}{\partial \tilde{\varepsilon}_{h_m}} = \sqrt{\frac{p_{z_S}^{TE}}{p_{z_R}^{TE}}} \left((-\delta_{Rm} + \delta_{Sm}) \frac{\mu_0}{4 p_{z_m}^{TE^2}} \mathcal{R}_B^{TE} + \frac{\partial \mathcal{R}_B^{TE}}{\partial \tilde{\varepsilon}_m} \right), \tag{43a}$$

$$\frac{\partial g_B^{TM}}{\partial \tilde{\varepsilon}_{h_m}} = \sqrt{\frac{p_{z_R}^{TM} \tilde{\varepsilon}_{h_S}}{p_{z_S}^{TM} \tilde{\varepsilon}_{h_R}}} \left(\frac{(-\delta_{Rm} + \delta_{Sm})}{2} \left(\frac{1}{\tilde{\varepsilon}_{h_m}} - \frac{\mu_0 - \frac{p_h^2}{\tilde{\varepsilon}_{v_m}}}{2 p_{z_m}^{TM^2}} \right) \mathcal{R}_B^{TM} + \frac{\partial \mathcal{R}_B^{TM}}{\partial \tilde{\varepsilon}_{h_m}} \right), \tag{43b}$$

$$\frac{\partial g_B^{TM}}{\partial \tilde{\varepsilon}_{v_m}} = \sqrt{\frac{p_{z_R}^{TM} \tilde{\varepsilon}_{h_S}}{p_{z_S}^{TM} \tilde{\varepsilon}_{h_R}}} \left((\delta_{Rm} - \delta_{Sm}) \frac{\tilde{\varepsilon}_{h_m} p_h^2}{4 \tilde{\varepsilon}_{v_m}^2 p_{z_m}^{TM^2}} \mathcal{R}_B^{TM} + \frac{\partial \mathcal{R}_B^{TM}}{\partial \tilde{\varepsilon}_{v_m}} \right), \tag{43c}$$

$$\frac{\partial g_C^{TE}}{\partial \tilde{\varepsilon}_{h_m}} = -\frac{\sqrt{p_{z_R}^{TE} p_{z_S}^{TE}}}{\mu_0} \left((\delta_{Rm} + \delta_{Sm}) \frac{\mu_0}{4 p_{z_m}^{TE^2}} \mathcal{R}_C^{TE} + \frac{\partial \mathcal{R}_C^{TE}}{\partial \tilde{\varepsilon}_{h_m}} \right), \tag{44a}$$

$$\frac{\partial g_C^{TM}}{\partial \tilde{\varepsilon}_{h_m}} = -\sqrt{\frac{\tilde{\varepsilon}_{h_R} \tilde{\varepsilon}_{h_S}}{p_{z_S}^{TM} p_{z_R}^{TM}}} \left(\frac{(\delta_{Rm} + \delta_{Sm})}{2} \left(\frac{1}{\tilde{\varepsilon}_{h_m}} - \frac{\mu_0 - \frac{p_h^2}{\tilde{\varepsilon}_{v_m}}}{2 p_{z_m}^{TM^2}} \right) \mathcal{R}_C^{TM} + \frac{\partial \mathcal{R}_C^{TM}}{\partial \tilde{\varepsilon}_{h_m}} \right), \tag{44b}$$

$$\frac{\partial g_C^{TM}}{\partial \tilde{\varepsilon}_{v_m}} = -\sqrt{\frac{\tilde{\varepsilon}_{h_R} \tilde{\varepsilon}_{h_S}}{p_{z_S}^{TM} p_{z_R}^{TM}}} \left(-(\delta_{Rm} + \delta_{Sm}) \frac{\tilde{\varepsilon}_{h_m} p_h^2}{4 \tilde{\varepsilon}_{v_m}^2 p_{z_m}^{TM^2}} \mathcal{R}_C^{TM} + \frac{\partial \mathcal{R}_C^{TM}}{\partial \tilde{\varepsilon}_{v_m}} \right). \tag{44c}$$

Using the expressions in eqs (41)–(44), we immediately obtain the derivatives of the Hankel integrals (eq. 3), for example,

$$\begin{aligned} \frac{\partial I_{X0}^{TE}}{\partial \tilde{\varepsilon}_{h_m}} &= \frac{\partial}{\partial \tilde{\varepsilon}_{h_m}} \left\{ \int_0^\infty \kappa J_0(\kappa r) g_X^{TE} \mathrm{d}\kappa \right\} \\ &= \int_0^\infty \kappa J_0(\kappa r) \frac{\partial g_X^{TE}}{\partial \tilde{\varepsilon}_{h_m}} \mathrm{d}\kappa. \end{aligned} \tag{45}$$

4.5 Derivatives of the EM field components

4.5.1 Horizontal electric dipole source

The EM field sensitivities to the horizontal medium properties $\tilde{\varepsilon}_{h_m}$ for an HED source can now be written as

$$\frac{\partial E_r}{\partial \tilde{\varepsilon}_{h_m}} = -\frac{I l_x}{4\pi} \cos\beta \left[\frac{\partial I_{A0}^{TM}}{\partial \tilde{\varepsilon}_{h_m}} + \frac{1}{r} \left(\frac{\partial I_{A1}^{TE}}{\partial \tilde{\varepsilon}_{h_m}} - \frac{\partial I_{A1}^{TM}}{\partial \tilde{\varepsilon}_{h_m}} \right) \right], \tag{46a}$$

$$\frac{\partial E_\theta}{\partial \tilde{\varepsilon}_{h_m}} = -\frac{I l_x}{4\pi} \sin\beta \left[-\frac{\partial I_{A0}^{TE}}{\partial \tilde{\varepsilon}_{h_m}} + \frac{1}{r} \left(\frac{\partial I_{A1}^{TE}}{\partial \tilde{\varepsilon}_{h_m}} - \frac{\partial I_{A1}^{TM}}{\partial \tilde{\varepsilon}_{h_m}} \right) \right], \tag{46b}$$

$$\frac{\partial E_z}{\partial \tilde{\varepsilon}_{h_m}} = \frac{Il_x}{4\pi}\frac{\mathrm{i}\cos\beta}{\omega\tilde{\varepsilon}_{v_R}}\int_0^\infty \kappa^2 J_1(\kappa r)\frac{\partial g_D^{TM}}{\partial \tilde{\varepsilon}_{h_m}}\mathrm{d}\kappa, \tag{46c}$$

$$\frac{\partial H_r}{\partial \tilde{\varepsilon}_{h_m}} = \frac{Il_x}{4\pi}\sin\beta\left[-\frac{\partial I_{D0}^{TE}}{\partial \tilde{\varepsilon}_{h_m}} + \frac{1}{r}\left(\frac{\partial I_{D1}^{TE}}{\partial \tilde{\varepsilon}_{h_m}} - \frac{\partial I_{D1}^{TM}}{\partial \tilde{\varepsilon}_{h_m}}\right)\right], \tag{46d}$$

$$\frac{\partial H_\theta}{\partial \tilde{\varepsilon}_{h_m}} = -\frac{Il_x}{4\pi}\cos\beta\left[\frac{\partial I_{D0}^{TM}}{\partial \tilde{\varepsilon}_{h_m}} + \frac{1}{r}\left(\frac{\partial I_{D1}^{TE}}{\partial \tilde{\varepsilon}_{h_m}} - \frac{\partial I_{D1}^{TM}}{\partial \tilde{\varepsilon}_{h_m}}\right)\right], \tag{46e}$$

$$\frac{\partial H_z}{\partial \tilde{\varepsilon}_{h_m}} = \frac{Il_x}{4\pi}\frac{\mathrm{i}\sin\beta}{\omega\mu_0}\int_0^\infty \kappa^2 J_1(\kappa r)\frac{\partial g_A^{TE}}{\partial \tilde{\varepsilon}_{h_m}}\mathrm{d}\kappa, \tag{46f}$$

where the derivatives of the integrals and kernels are given by eqs (45), (41a), (41b), (42a) and (42b).

The sensitivities to the vertical medium properties $\tilde{\varepsilon}_{v_m}$ are

$$\frac{\partial E_r}{\partial \tilde{\varepsilon}_{v_m}} = -\frac{Il_x}{4\pi}\cos\beta\left[\frac{\partial I_{A0}^{TM}}{\partial \tilde{\varepsilon}_{v_m}} - \frac{1}{r}\frac{\partial I_{A1}^{TM}}{\partial \tilde{\varepsilon}_{v_m}}\right], \tag{47a}$$

$$\frac{\partial E_\theta}{\partial \tilde{\varepsilon}_{v_m}} = -\frac{Il_x}{4\pi}\sin\beta\left[-\frac{1}{r}\frac{\partial I_{A1}^{TM}}{\partial \tilde{\varepsilon}_{v_m}}\right], \tag{47b}$$

$$\frac{\partial E_z}{\partial \tilde{\varepsilon}_{v_m}} = \delta_{Rm}\left(-\frac{Il_x}{4\pi}\frac{\mathrm{i}\cos\beta}{\omega\tilde{\varepsilon}_{v_R}^2}\int_0^\infty \kappa^2 J_1(\kappa r) g_D^{TM}\mathrm{d}\kappa\right) + \frac{Il_x}{4\pi}\frac{\mathrm{i}\cos\beta}{\omega\tilde{\varepsilon}_{v_R}}\int_0^\infty \kappa^2 J_1(\kappa r)\frac{\partial g_D^{TM}}{\partial \tilde{\varepsilon}_{v_m}}\mathrm{d}\kappa, \tag{47c}$$

$$\frac{\partial H_r}{\partial \tilde{\varepsilon}_{v_m}} = \frac{Il_x}{4\pi}\sin\beta\left[-\frac{1}{r}\frac{\partial I_{D1}^{TM}}{\partial \tilde{\varepsilon}_{v_m}}\right], \tag{47d}$$

$$\frac{\partial H_\theta}{\partial \tilde{\varepsilon}_{v_m}} = -\frac{Il_x}{4\pi}\cos\beta\left[\frac{\partial I_{D0}^{TM}}{\partial \tilde{\varepsilon}_{v_m}} - \frac{1}{r}\frac{\partial I_{D1}^{TM}}{\partial \tilde{\varepsilon}_{v_m}}\right], \tag{47e}$$

$$\frac{\partial H_z}{\partial \tilde{\varepsilon}_{v_m}} = 0, \tag{47f}$$

with the derivatives of the integral kernels given by eqs. (41c) and (42c).

4.5.2 Horizontal magnetic dipole source

For an HMD source, we obtain the EM field sensitivities with respect to $\tilde{\varepsilon}_{h_m}$

$$\frac{\partial E_r}{\partial \tilde{\varepsilon}_{h_m}} = -\frac{\mathrm{i}\omega\mu_0 I a_x}{4\pi}\sin\beta\left[\frac{\partial I_{B0}^{TM}}{\partial \tilde{\varepsilon}_{h_m}} + \frac{1}{r}\left(\frac{\partial I_{B1}^{TE}}{\partial \tilde{\varepsilon}_{h_m}} - \frac{\partial I_{B1}^{TM}}{\partial \tilde{\varepsilon}_{h_m}}\right)\right], \tag{48a}$$

$$\frac{\partial E_\theta}{\partial \tilde{\varepsilon}_{h_m}} = \frac{\mathrm{i}\omega\mu_0 I a_x}{4\pi}\cos\beta\left[-\frac{\partial I_{B0}^{TE}}{\partial \tilde{\varepsilon}_{h_m}} + \frac{1}{r}\left(\frac{\partial I_{B1}^{TE}}{\partial \tilde{\varepsilon}_{h_m}} - \frac{\partial I_{B1}^{TM}}{\partial \tilde{\varepsilon}_{h_m}}\right)\right], \tag{48b}$$

$$\frac{\partial E_z}{\partial \tilde{\varepsilon}_{h_m}} = -\frac{I a_x}{4\pi}\frac{\mu_0}{\tilde{\varepsilon}_{v_R}}\sin\beta\int_0^\infty \kappa^2 J_1(\kappa r)\frac{\partial g_C^{TM}}{\partial \tilde{\varepsilon}_{h_m}}\mathrm{d}\kappa, \tag{48c}$$

$$\frac{\partial H_r}{\partial \tilde{\varepsilon}_{h_m}} = -\frac{\mathrm{i}\omega\mu_0 I a_x}{4\pi}\cos\beta\left[-\frac{\partial I_{C0}^{TE}}{\tilde{\varepsilon}_{h_m}} + \frac{1}{r}\left(\frac{\partial I_{C1}^{TE}}{\partial \tilde{\varepsilon}_{h_m}} - \frac{\partial I_{C1}^{TM}}{\partial \tilde{\varepsilon}_{h_m}}\right)\right], \tag{48d}$$

$$\frac{\partial H_\theta}{\partial \tilde{\varepsilon}_{h_m}} = -\frac{\mathrm{i}\omega\mu_0 I a_x}{4\pi}\sin\beta\left[\frac{\partial I_{C0}^{TM}}{\partial \tilde{\varepsilon}_{h_m}} + \frac{1}{r}\left(\frac{\partial I_{C1}^{TE}}{\partial \tilde{\varepsilon}_{h_m}} - \frac{\partial I_{C1}^{TM}}{\partial \tilde{\varepsilon}_{h_m}}\right)\right], \tag{48e}$$

$$\frac{\partial H_z}{\partial \tilde{\varepsilon}_{h_m}} = \frac{I a_x}{4\pi}\cos\beta\int_0^\infty \kappa^2 J_1(\kappa r)\frac{\partial g_B^{TE}}{\partial \tilde{\varepsilon}_{h_m}}\mathrm{d}\kappa, \tag{48f}$$

with the derivatives of the integrals and kernels given by eqs (45), (43a), (43b), (44a) and (44b).

The sensitivities with respect to $\tilde{\varepsilon}_{v_m}$ are

$$\frac{\partial E_r}{\partial \tilde{\varepsilon}_{v_m}} = -\frac{\mathrm{i}\omega\mu_0 I a_x}{4\pi}\sin\beta\left[\frac{\partial I_{B0}^{TM}}{\partial \tilde{\varepsilon}_{v_m}} - \frac{1}{r}\frac{\partial I_{B1}^{TM}}{\partial \tilde{\varepsilon}_{v_m}}\right], \tag{49a}$$

$$\frac{\partial E_\theta}{\partial \tilde{\varepsilon}_{v_m}} = \frac{\mathrm{i}\omega\mu_0 I a_x}{4\pi}\cos\beta\left[-\frac{1}{r}\frac{\partial I_{B1}^{TM}}{\partial \tilde{\varepsilon}_{v_m}}\right], \tag{49b}$$

$$\frac{\partial E_z}{\partial \tilde{\varepsilon}_{v_m}} = \delta_{Rm}\left(\frac{Ia_x}{4\pi}\frac{\mu_0}{\tilde{\varepsilon}^2_{v_R}}\sin\beta\int_0^\infty \kappa^2 J_1(\kappa r) g_C^{TM}\mathrm{d}\kappa\right) - \frac{Ia_x}{4\pi}\frac{\mu_0}{\tilde{\varepsilon}_{v_R}}\sin\beta\int_0^\infty \kappa^2 J_1(\kappa r)\frac{\partial g_C^{TM}}{\partial \tilde{\varepsilon}_{v_m}}\mathrm{d}\kappa, \tag{49c}$$

$$\frac{\partial H_r}{\partial \tilde{\varepsilon}_{v_m}} = -\frac{\mathrm{i}\omega\mu_0 Ia_x}{4\pi}\cos\beta\left[-\frac{1}{r}\frac{\partial I_{C1}^{TM}}{\partial \tilde{\varepsilon}_{v_m}}\right], \tag{49d}$$

$$\frac{\partial H_\theta}{\partial \tilde{\varepsilon}_{v_m}} = -\frac{\mathrm{i}\omega\mu_0 Ia_x}{4\pi}\sin\beta\left[\frac{\partial I_{C0}^{TM}}{\partial \tilde{\varepsilon}_{v_m}} - \frac{1}{r}\frac{\partial I_{C1}^{TM}}{\partial \tilde{\varepsilon}_{v_m}}\right], \tag{49e}$$

$$\frac{\partial H_z}{\partial \tilde{\varepsilon}_{v_m}} = 0, \tag{49f}$$

with the derivatives of the integral kernels given in eqs. (43c) and (44c).

4.5.3 Vertical electric dipole source

The EM field sensitivities for a VED source with respect to $\tilde{\varepsilon}_{h_m}$ are

$$\frac{\partial E_r}{\partial \tilde{\varepsilon}_{h_m}} = \frac{Il_z}{4\pi}\frac{\mathrm{i}}{\omega\tilde{\varepsilon}_{v_S}}\int_0^\infty \kappa^2 J_1(\kappa r)\frac{\partial g_B^{TM}}{\partial \tilde{\varepsilon}_{h_m}}\mathrm{d}\kappa, \tag{50a}$$

$$\frac{\partial E_z}{\partial \tilde{\varepsilon}_m} = -\frac{Il_z}{4\pi}\frac{1}{\omega^2\tilde{\varepsilon}_{v_R}\tilde{\varepsilon}_{v_S}}\int_0^\infty \kappa^3 J_0(\kappa r)\frac{\partial g_C^{TM}}{\partial \tilde{\varepsilon}_{h_m}}\mathrm{d}\kappa, \tag{50b}$$

$$\frac{\partial H_\theta}{\partial \tilde{\varepsilon}_{h_m}} = \frac{Il_z}{4\pi}\frac{\mathrm{i}}{\omega\tilde{\varepsilon}_{v_S}}\int_0^\infty \kappa^2 J_1(\kappa r)\frac{\partial g_C^{TM}}{\partial \tilde{\varepsilon}_{h_m}}\mathrm{d}\kappa, \tag{50c}$$

where the derivatives of the integral kernels are given in eqs (43b) and (44b).

The sensitivities with respect to $\tilde{\varepsilon}_{v_m}$ are

$$\frac{\partial E_r}{\partial \tilde{\varepsilon}_{v_m}} = \delta_{Sm}\left(-\frac{Il_z}{4\pi}\frac{\mathrm{i}}{\omega\tilde{\varepsilon}^2_{v_S}}\int_0^\infty \kappa^2 J_1(\kappa r) g_B^{TM}\mathrm{d}\kappa\right) + \frac{Il_z}{4\pi}\frac{\mathrm{i}}{\omega\tilde{\varepsilon}_{v_S}}\int_0^\infty \kappa^2 J_1(\kappa r)\frac{\partial g_B^{TM}}{\partial \tilde{\varepsilon}_{v_m}}\mathrm{d}\kappa, \tag{51a}$$

$$\begin{aligned}\frac{\partial E_z}{\partial \tilde{\varepsilon}_{v_m}} = {} & \left(\frac{\delta_{Sm}}{\tilde{\varepsilon}_{v_S}} + \frac{\delta_{Rm}}{\tilde{\varepsilon}_{v_R}}\right)\left(\frac{Il_z}{4\pi}\frac{1}{\omega^2\tilde{\varepsilon}_{v_R}\tilde{\varepsilon}_{v_S}}\int_0^\infty \kappa^3 J_0(\kappa r) g_C^{TM}\mathrm{d}\kappa\right) \\ & -\frac{Il_z}{4\pi}\frac{1}{\omega^2\tilde{\varepsilon}_{v_R}\tilde{\varepsilon}_{v_S}}\int_0^\infty \kappa^3 J_0(\kappa r)\frac{\partial g_C^{TM}}{\partial \tilde{\varepsilon}_{v_m}}\mathrm{d}\kappa - \delta_{Sm}\left(\frac{Il_z}{4\pi}\frac{1}{\mathrm{i}\omega\tilde{\varepsilon}^2_{v_S}}\delta(x)\delta(y)\delta(z-z_s)\right),\end{aligned} \tag{51b}$$

$$\frac{\partial H_\theta}{\partial \tilde{\varepsilon}_{v_m}} = \delta_{Sm}\left(-\frac{Il_z}{4\pi}\frac{\mathrm{i}}{\omega\tilde{\varepsilon}^2_{v_S}}\int_0^\infty \kappa^2 J_1(\kappa r) g_C^{TM}\mathrm{d}\kappa\right) + \frac{Il_z}{4\pi}\frac{\mathrm{i}}{\omega\tilde{\varepsilon}_{v_S}}\int_0^\infty \kappa^2 J_1(\kappa r)\frac{\partial g_C^{TM}}{\partial \tilde{\varepsilon}_{v_m}}\mathrm{d}\kappa, \tag{51c}$$

with the derivatives of the integral kernels given in eqs (43c) and (44c).

4.5.4 Vertical magnetic dipole source

For a VMD source, we obtain the EM field sensitivities with respect to $\tilde{\varepsilon}_{h_m}$

$$\frac{\partial E_\theta}{\partial \tilde{\varepsilon}_{h_m}} = -\frac{Ia_z}{4\pi}\int_0^\infty \kappa^2 J_1(\kappa r)\frac{\partial g_A^{TE}}{\partial \tilde{\varepsilon}_{h_m}}\mathrm{d}\kappa, \tag{52a}$$

$$\frac{\partial H_r}{\partial \tilde{\varepsilon}_{h_m}} = \frac{Ia_z}{4\pi}\int_0^\infty \kappa^2 J_1(\kappa r)\frac{\partial g_D^{TE}}{\partial \tilde{\varepsilon}_{h_m}}\mathrm{d}\kappa, \tag{52b}$$

$$\frac{\partial H_z}{\partial \tilde{\varepsilon}_{h_m}} = \frac{Ia_z}{4\pi}\frac{\mathrm{i}}{\omega\mu_0}\int_0^\infty \kappa^3 J_0(\kappa r)\frac{\partial g_A^{TE}}{\partial \tilde{\varepsilon}_{h_m}}\mathrm{d}\kappa, \tag{52c}$$

with the integral kernel derivatives given in eqs (41a) and (42a). Sensitivities with respect to $\tilde{\varepsilon}_{v_m}$ are zero, because VMD sources generate pure TE-mode fields.

4.5.5 Long horizontal wire source

As for point dipole sources, the EM field sensitivities for finite-length horizontal electrical sources are obtained by differentiating the integral kernels. For $\tilde{\varepsilon}_{h_m}$,

$$\frac{\partial E_x}{\partial \tilde{\varepsilon}_{h_m}} = \frac{I}{4\pi}\sum_{n=1}^{N}\Delta x\int_0^\infty -\kappa\frac{\partial g_A^{TE}}{\partial \tilde{\varepsilon}_{h_m}}J_0(\kappa r_n)\,\mathrm{d}\kappa - \frac{I}{4\pi}\sum_{n=1}^{2}(-1)^n\frac{x-x_n^S}{r_n^S}\int_0^\infty\left[\frac{\partial g_A^{TE}}{\partial \tilde{\varepsilon}_{h_m}}-\frac{\partial g_A^{TM}}{\partial \tilde{\varepsilon}_{h_m}}\right]J_1\left(\kappa r_n^S\right)\mathrm{d}\kappa, \tag{53a}$$

$$\frac{\partial E_y}{\partial \tilde{\varepsilon}_{h_m}} = -\frac{I}{4\pi}\sum_{n=1}^{2}(-1)^n\frac{y}{r_n^S}\int_0^\infty\left[\frac{\partial g_A^{TE}}{\partial \tilde{\varepsilon}_{h_m}}-\frac{\partial g_A^{TM}}{\partial \tilde{\varepsilon}_{h_m}}\right]J_1\left(\kappa r_n^S\right)\mathrm{d}\kappa, \tag{53b}$$

$$\frac{\partial E_z}{\partial \tilde{\varepsilon}_{h_m}} = \frac{\mathrm{i}I}{4\pi\omega\tilde{\varepsilon}_{v_R}}\sum_{n=1}^{2}(-1)^n\int_0^\infty\kappa\frac{\partial g_D^{TM}}{\partial \tilde{\varepsilon}_{h_m}}J_0\left(\kappa r_n^S\right)\mathrm{d}\kappa, \tag{53c}$$

$$\frac{\partial H_x}{\partial \tilde{\varepsilon}_{h_m}} = \frac{I}{4\pi}\sum_{n=1}^{2}(-1)^n\frac{y}{r_n^S}\int_0^\infty\left[\frac{\partial g_D^{TE}}{\partial \tilde{\varepsilon}_{h_m}}-\frac{\partial g_D^{TM}}{\partial \tilde{\varepsilon}_{h_m}}\right]J_1\left(\kappa r_n^S\right)\mathrm{d}\kappa, \tag{53d}$$

$$\frac{\partial H_y}{\partial \tilde{\varepsilon}_{h_m}} = \frac{I}{4\pi}\sum_{n=1}^{N}\Delta x\int_0^\infty -\kappa\frac{\partial g_D^{TE}}{\partial \tilde{\varepsilon}_{h_m}}J_0(\kappa r_n)\,\mathrm{d}\kappa - \frac{I}{4\pi}\sum_{n=1}^{2}(-1)^n\frac{x-x_n^S}{r_n^S}\int_0^\infty\left[\frac{\partial g_D^{TE}}{\partial \tilde{\varepsilon}_{h_m}}-\frac{\partial g_D^{TM}}{\partial \tilde{\varepsilon}_{h_m}}\right]J_1\left(\kappa r_n^S\right)\mathrm{d}\kappa, \tag{53e}$$

$$\frac{\partial H_z}{\partial \tilde{\varepsilon}_{h_m}} = \frac{\mathrm{i}Iy}{4\pi\mu_0\omega}\sum_{n=1}^{N}\frac{\Delta x}{r_n}\int_0^\infty\kappa^2\frac{\partial g_A^{TE}}{\partial \tilde{\varepsilon}_{h_m}}J_1(\kappa r_n)\,\mathrm{d}\kappa. \tag{53f}$$

The sensitivities with respect to $\tilde{\varepsilon}_{v_m}$ are

$$\frac{\partial E_x}{\partial \tilde{\varepsilon}_{v_m}} = -\frac{I}{4\pi}\sum_{n=1}^{2}(-1)^n\frac{x-x_n^S}{r_n^S}\int_0^\infty-\frac{\partial g_A^{TM}}{\partial \tilde{\varepsilon}_{v_m}}J_1\left(\kappa r_n^S\right)\mathrm{d}\kappa, \tag{54a}$$

$$\frac{\partial E_y}{\partial \tilde{\varepsilon}_{v_m}} = -\frac{I}{4\pi}\sum_{n=1}^{2}(-1)^n\frac{y}{r_n^S}\int_0^\infty-\frac{\partial g_A^{TM}}{\partial \tilde{\varepsilon}_{v_m}}J_1\left(\kappa r_n^S\right)\mathrm{d}\kappa, \tag{54b}$$

$$\frac{\partial E_z}{\partial \tilde{\varepsilon}_{v_m}} = \delta_{Rm}\left(-\frac{\mathrm{i}I}{4\pi\omega\tilde{\varepsilon}_{v_R}^2}\sum_{n=1}^{2}(-1)^n\int_0^\infty\kappa g_D^{TM}J_0\left(\kappa r_n^S\right)\mathrm{d}\kappa\right) + \frac{\mathrm{i}I}{4\pi\omega\tilde{\varepsilon}_{v_R}}\sum_{n=1}^{2}(-1)^n\int_0^\infty\kappa\frac{\partial g_D^{TM}}{\partial \tilde{\varepsilon}_{v_m}}J_0\left(\kappa r_n^S\right)\mathrm{d}\kappa, \tag{54c}$$

$$\frac{\partial H_x}{\partial \tilde{\varepsilon}_{v_m}} = \frac{I}{4\pi}\sum_{n=1}^{2}(-1)^n\frac{y}{r_n^S}\int_0^\infty-\frac{\partial g_D^{TM}}{\partial \tilde{\varepsilon}_{v_m}}J_1\left(\kappa r_n^S\right)\mathrm{d}\kappa, \tag{54d}$$

$$\frac{\partial H_y}{\partial \tilde{\varepsilon}_{v_m}} = -\frac{I}{4\pi}\sum_{n=1}^{2}(-1)^n\frac{x-x_n^S}{r_n^S}\int_0^\infty-\frac{\partial g_D^{TM}}{\partial \tilde{\varepsilon}_{v_m}}J_1\left(\kappa r_n^S\right)\mathrm{d}\kappa, \tag{54e}$$

$$\frac{\partial H_z}{\partial \tilde{\varepsilon}_{v_m}} = 0. \tag{54f}$$

5 VERIFICATION AND EXAMPLES

5.1 Example 1: Marine CSEM survey

5.1.1 Comparison to numerical solutions

We verify our analytical solutions against numerical sensitivity computations. To demonstrate the validity of the solutions for a general case in which all of the terms contributing to the reflection and transmission response derivatives assume non-zero values, we use the five-layer conductivity model displayed in Fig. 3. This is a typical marine CSEM model; the layers represent air, water and seafloor sediments with an embedded hydrocarbon-bearing thin resistor. The horizontal and vertical conductivities are equal, and we evaluate sensitivities with respect to $\ln \sigma_h$ and $\ln \sigma_v$, assuming VTI-anisotropy, and with respect to isotropic $\ln \sigma$. Permittivity is set to $\varepsilon_r = 1$ in the entire model. At the low frequencies considered, its influence is negligible in all layers except for the air. Sources are placed 30 m above the seafloor ($z = 270$ m) and a line of 151 receivers is located at the seafloor ($z = 299.9$ m). Quasi-analytical solutions are obtained using the fast Hankel transform algorithm of Chave (1983). In the vertical column above and beneath the source point ($r = 0$), the Hankel integrals simplify and are evaluated using adaptive integration routines from the QUADPACK library (Piessens *et al.* 1983). Accurate numerical results are obtained using Ridders' numerical differentiation algorithm (Ridders 1982; Press *et al.* 1992).

Fig. 4 shows sensitivities to the water and sedimentary layers for all source types (sensitivities to air are zeroed by taking derivatives with respect to $\ln \sigma_m$, see eq. 13). The analytical and numerical solutions agree very well for all source types and layers. Relative differences are mostly on the order of 10^{-4} or less. For layers exhibiting very low sensitivities (e.g. the reservoir for the HED and HMD sources and σ_h sensitivity (Fig. 4a and e) and the water for the HMD source and σ_v sensitivity (Fig. 4f)), the numerical solution is somewhat noisy, whereas the analytical solution is smooth and clearly superior to the numerical one.

The computation of the numerical results shown in Fig. 4 required 92 and 44 forward modelling runs for VTI and isotropic conductivities, respectively, and took 29.9 and 13.3 s on a 2.83 GHz quad-core CPU. The analytical VTI and isotropic calculations only took 2.5 and 2.1 s, respectively. There is a significant increase of runtime for numerical VTI over isotropic computations, because numerical VTI computations require approximately twice as many modelling runs as isotropic calculations. In contrast, analytical VTI sensitivity evaluations require relatively little additional effort compared to isotropic calculations. VTI computation for σ_h is as expensive as isotropic computation, and only a few extra TM-mode integral evaluations are required for computing σ_v sensitivities (see eqs. 47, 49, 51 and 54).

The savings in computational time increase significantly with increasing number of layers (Fig. 5), demonstrating that using the analytical expressions will be particularly advantageous within inversion algorithms. Also, the efficiency gain of analytical over numerical computations

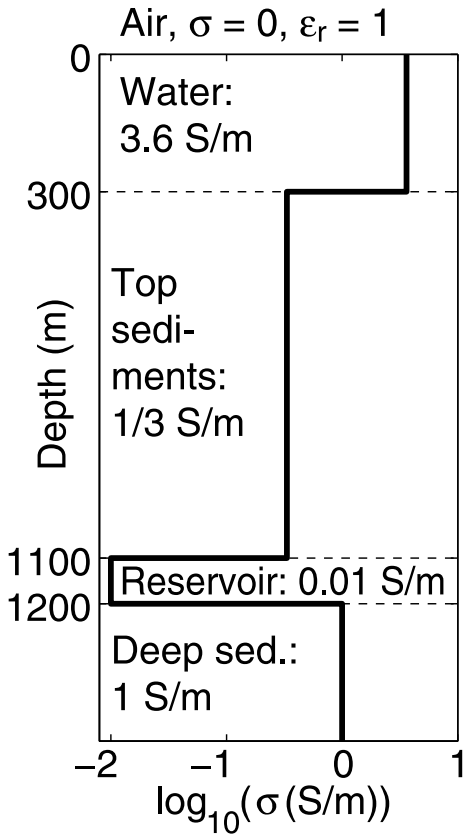

Figure 3. Marine CSEM model used for comparing analytical and numerical sensitivities.

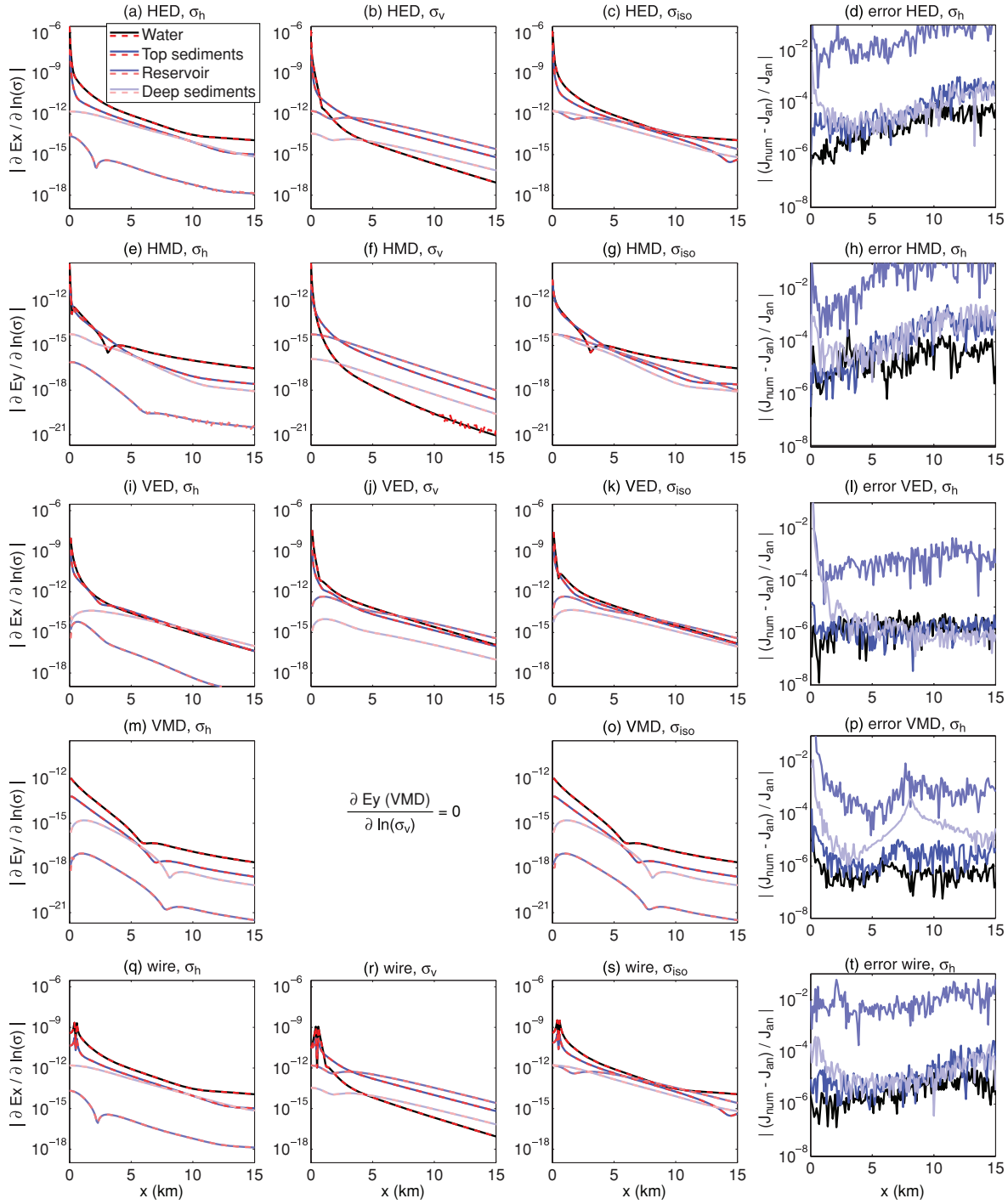

Figure 4. Comparison of sensitivities computed quasi-analytically and numerically, for the non-air layers of the model displayed in Fig. 3 and (a–d) HED, (e–h) HMD, (i–l) VED, (m–p) VMD sources located at $(x, y, z) = (0, 0, 270)$ m and (q–t) a 1-km long x-directed finite wire source centred at $(x, y, z) = (0, 0, 270)$ m. Sensitivities are normalized to the source length. Sensitivities J_{Ex_m} (see eq. 13) are shown for the electric and sensitivities J_{Ey_m} for the magnetic sources. Receivers are located at the seafloor ($z = 299.9$ m), frequency is 0.5 Hz. The three columns to the left show absolute values of sensitivity to the horizontal, vertical and isotropic conductivity, respectively. Blue lines indicate analytical and red dashed lines indicate numerical results. The right column shows relative errors between analytical and numerical results for the horizontal conductivity.

is consistently larger for VTI media than for homogeneous ones (Figs 5b and c). Obviously, straightforward finite-difference computations conducted using, for EM field component F,

$$\frac{\partial F}{\partial \sigma_m} \approx \frac{F(\sigma_m + \Delta\sigma_m) - F(\sigma_m)}{\Delta\sigma_m},$$

would require significantly less computational effort than using Ridders' algorithm for numerical differentiation. However, finite-difference computations must be expected to be of limited accuracy because of the non-linear dependency of the EM field on conductivity.

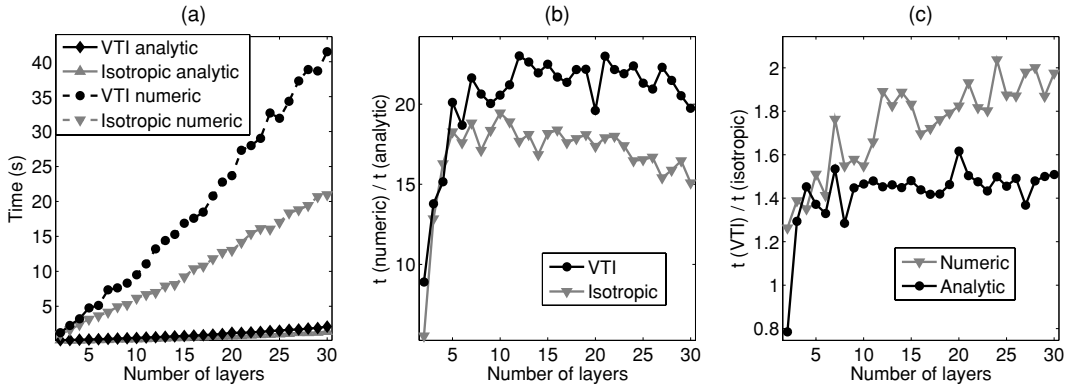

Figure 5. Computation times for analytical and numerical sensitivity evaluation in dependence of the number of layers. We display (a) runtimes for numerical and analytical VTI and isotropic calculations for an HED source and a line of 151 receivers, (b) the ratios between the numerical and analytical computation times and (c) the ratios between the runtimes for VTI and isotropic calculations.

5.1.2 Interpretation

Fig. 4 also demonstrates sensitivity characteristics for a typical marine CSEM survey. The sensitivity values for the electric unit sources generally exceed those for the magnetic unit sources by several orders of magnitude. This amplitude behaviour is similar to that of EM fields for electric and magnetic sources. It indicates that magnetic sources have to be stronger than electric ones to obtain subsurface responses of comparable amplitudes. Sensitivities for the long wire source (normalized to the source length) are very similar to those for the HED, except for short distances, where maxima occur, respectively, at the HED location and the end points of the long source. Sensitivity to the vertical conductivity of the water is comparatively low for all horizontal sources, probably due to the primarily horizontal current flow generated in the water. Sensitivity to the horizontal conductivity of the reservoir layer is also very low for all sources. Sensitivity to the vertical reservoir conductivity is much higher and nearly comparable to the σ_v sensitivities for the water and the other sedimentary layers. This demonstrates that hydrocarbon reservoir detectability primarily hinges on the vertical reservoir conductivity.

Notably, the fields generated by an HMD source located in the water are sensitive both to the horizontal and vertical conductivity structure (Figs 4e and f), similar to the fields generated by an HED, since both sources generate fields of similar behaviour at the seafloor (Chave 2009). In contrast, magnetic sources located above the surface can only couple to the ground inductively, that is, they induce horizontal currents (e.g. Chave & Cox 1982; Ferguson & Edwards 1994) and are therefore only sensitive to the horizontal conductivity.

For the isotropic model used in Fig. 4, the isotropic sensitivities are the sums of the sensitivities to the horizontal and vertical conductivities. This is mathematically easily understood; taking derivatives with respect to either σ_{h_m} or σ_{v_m} only comprises differentiation with respect to part of the occurrences of conductivity in the EM field expressions. General additive properties of the derivatives then imply

$$\frac{\partial F}{\partial \sigma_m} = \frac{\partial F}{\partial \sigma_{h_m}} + \frac{\partial F}{\partial \sigma_{v_m}}, \quad \text{for} \quad \sigma_{h_m} = \sigma_{v_m} = \sigma_m. \tag{55}$$

5.2 Example 2: Sensitivities to thin layers for land CSEM surveying

We now apply analytical sensitivity calculations for studying the feasibility of land CSEM exploration and monitoring of thin resistive layers representative of carbon dioxide storage reservoirs. We do not attempt at conducting an exhaustive feasibility study. Rather, we present several examples demonstrating the computation of sensitivities for various realistic source–receiver geometries. We use the layered model displayed in Fig. 6. This model roughly represents the geology at the Ketzin CO_2 injection test site located east of Berlin, Germany. The thin resistive reservoir layer has the actual depth and thickness, and resistivity similar to that of the CO_2-bearing sandstone at the site (Giese *et al.* 2009). Initially, we assume equal horizontal and vertical conductivities.

In Fig. 7, we display E_x sensitivities to $\ln \sigma_h$ and $\ln \sigma_v$ for the three layers of this model and a wide frequency range. Receivers are located on a 20-km long SSE–NNW directed line at depth 0.05 m, representing buried electric field sensors. The orientation of the receiver line was chosen according to geology and logistical constraints at the site. The source is a grounded HED located at $(x, y, z) = (0, 0, 0.1)$ m and oriented parallel to the receiver line. Sensitivities were computed using eqs (46) and (47), with rotations to account for the source orientation.

For display purposes, we normalize the sensitivities by the absolute values of the EM field. This effectively converts the sensitivities to relative quantities, as can be seen by rewriting the sensitivity to field component F (see eq. 13) using the formal definition of derivatives:

$$J_{F_m} = \left(\lim_{\delta\sigma_m \to 0} \frac{F(\sigma_m + \delta\sigma_m) - F(\sigma_m)}{\delta\sigma_m} \right) \frac{\partial \sigma_m}{\partial \ln \sigma_m}. \tag{56}$$

Here, the numerator contains the overall difference between fields for slightly different conductivities. Normalizing by $|F|$ and taking $|J_{F_m}|$

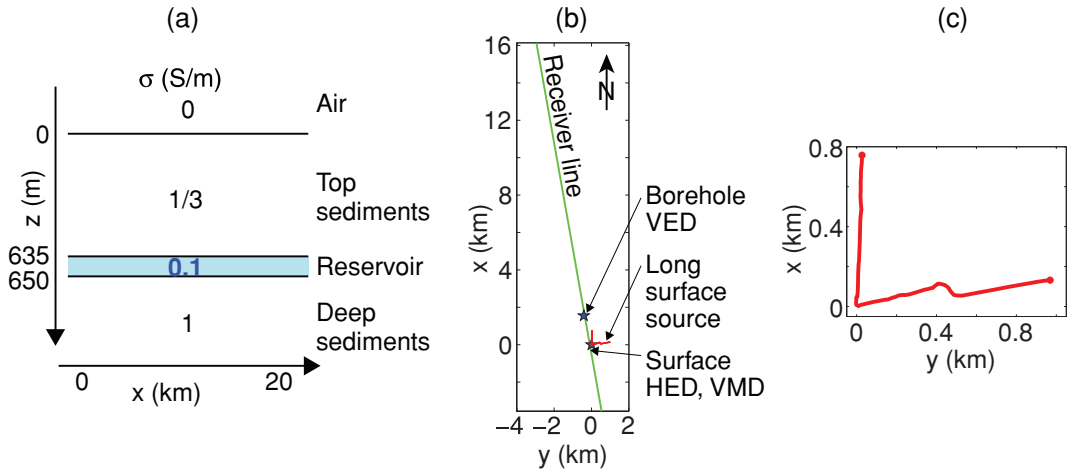

Figure 6. (a) 1-D conductivity model roughly representing the geology at the Ketzin carbon sequestration site. (b) Top view of the source–receiver geometries used for feasibility studies. (c) Close-up of the long grounded surface source.

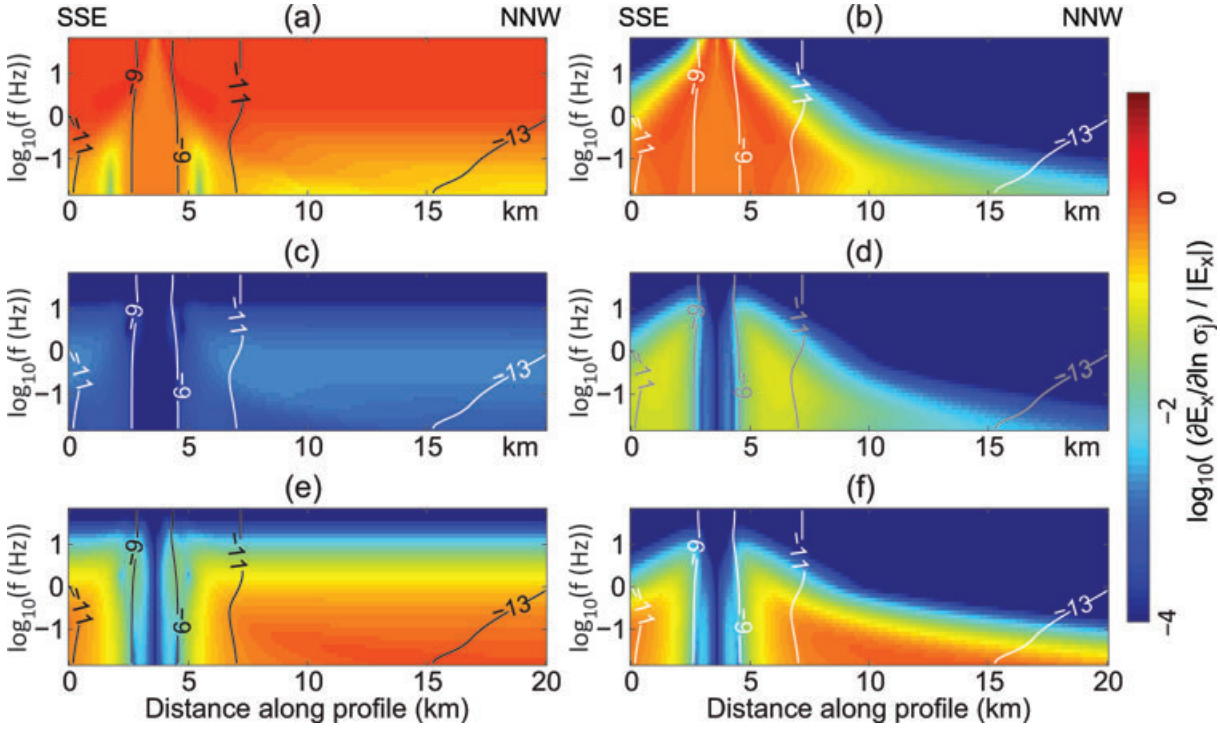

Figure 7. E_x sensitivity to the (a, b) top sediments, (c, d) reservoir layer and (e, f) deep sediments of the model shown in Fig. 6(a), for a 20-km long line of surface receivers, a surface HED source parallel to the receiver line located at $(x, y) = (0, 0)$ m, and frequencies between 1/64 and 64 Hz. The left and right columns show sensitivities to horizontal and vertical conductivity, respectively. Sensitivities are normalized by $|E_x|$. Contours indicate E_x amplitudes as $\log_{10}|E_x|$.

leads to

$$\frac{|J_{F_m}|}{|F|} = \left(\lim_{\delta\sigma_m \to 0} \frac{|F(\sigma_m + \delta\sigma_m) - F(\sigma_m)|}{|F(\sigma_m)||\delta\sigma_m|} \right) \frac{\partial \sigma_m}{\partial \ln \sigma_m}. \tag{57}$$

This corresponds closely to the relative amplitude difference between fields for a finite conductivity change. As measurement accuracy is typically on the order of a small percentage of the measured field, regardless of the absolute field values (e.g. Ziolkowski *et al.* 2010), normalized sensitivities are better indicators of target detectability than absolute ones as long as absolute amplitudes are measurable.

Sensitivity to the horizontal conductivity of the top sediments is high over the entire distance range, whereas sensitivity to the vertical conductivity of the top layer is maximum near the source and decreases steadily with increasing source–receiver distance and frequency (Figs 7a and b). As for the marine CSEM example, sensitivity to the horizontal reservoir conductivity is insignificantly low, whereas sensitivity to the vertical reservoir conductivity approaches that of the top and bottom sediments, attaining a maximum for frequencies near 0.25 Hz and source–receiver offsets near 2.5 km. Sensitivity to the deep sediments (Figs 7e and f) expectedly increases with decreasing frequency, and the

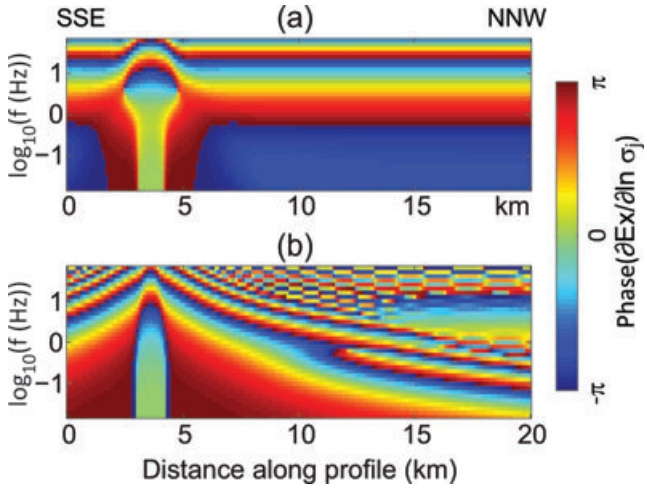

Figure 8. Phases of the E_x sensitivities to the (a) horizontal and (b) vertical conductivity of the reservoir layer, for the same source–receiver configuration as used in Fig. 7.

deep layer is not seen at near source–receiver offsets. As for the top sedimentary layer, sensitivity to σ_v varies more strongly with frequency and distance than sensitivity to σ_h.

In principle, the phase of the sensitivity should provide additional information on target characteristics and detectability. However, phases of the sensitivity may vary rapidly and contain frequent cycle skips (Fig. 8), and are therefore difficult to interpret. Variations of the phases of the σ_h and σ_v sensitivities to the reservoir coincide with the respective amplitude variations (compare Figs 8 to 7b and d). Within a narrow region near the source at low frequencies, phases are nearly zero, suggesting that we effectively are in the direct-current regime here.

In Fig. 9, we display electric and magnetic field sensitivities for the long grounded wire source depicted in Fig. 6(c). This source has been used for CSEM measurements at the site. It was modelled as a set of finite-length horizontal wire segments. For each segment, sensitivities were computed using eqs (53) and (54), and total sensitivity was obtained by integrating over all wire segments. The E_x sensitivity pattern (Fig. 9a) is similar to that of the HED (see Fig. 7d), yet slightly distorted due to the irregular source geometry. Magnetic field sensitivity to the resistive reservoir is insignificantly low, as is shown in Fig. 9(b) for the example of H_y. This indicates that the magnetic field would not be useful for imaging this resistive reservoir. In contrast, magnetic field sensitivity is significantly higher for conductive layers. Fig. 9(c) illustrates this for the horizontal conductivity of the reservoir increased to 2.5 S m^{-1}.

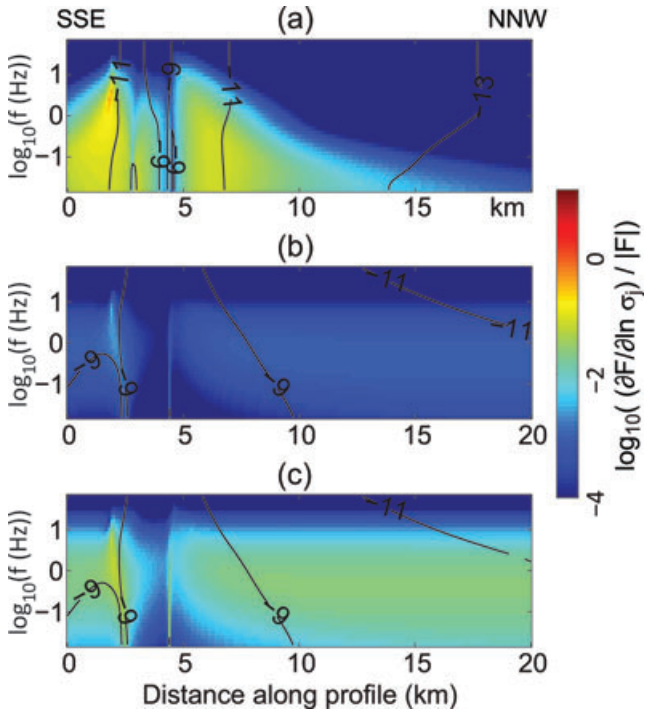

Figure 9. (a) E_x sensitivity to σ_v and (b) H_y sensitivity to σ_h of the reservoir layer in Fig. 6(a), normalized by E_x and H_y amplitudes, for the long grounded wire source depicted in Fig. 6(c). (c) shows H_y sensitivity to σ_h for σ_h of the thin layer increased to 2.5 S m^{-1}.

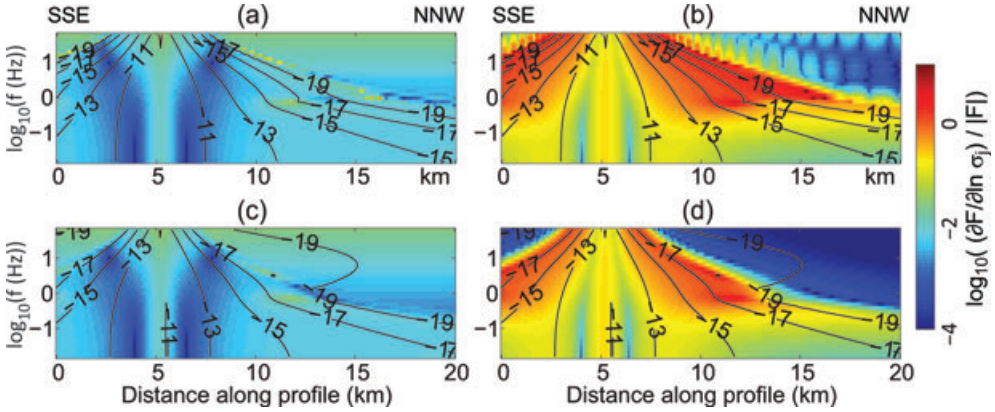

Figure 10. Sensitivity to the reservoir layer of Fig. 6(a), normalized by EM field amplitudes, for the VED source depicted in Fig. 6(b). Shown are E_x sensitivity to (a) σ_h and (b) σ_v and H_y sensitivity to (c) σ_h and (d) σ_v.

Sensitivities for a vertical borehole source are shown in Fig. 10. The source location (Fig. 6b) corresponds to the position of the observation well Ktzi200 present at the site (Giese *et al.* 2009), and its depth of 670 m, slightly below the reservoir layer, corresponds to the centre of a borehole electrode array installed in the well for DC resistivity measurements. Sensitivities for this source were computed using eqs (50) and (51).

Normalized sensitivity to the horizontal and vertical reservoir conductivity is much higher for the borehole VED source than for the surface sources. As for the surface sources, electric field sensitivity to σ_v is significantly higher than that to σ_h. However, EM field amplitudes are much lower than for the surface sources, and normalized sensitivity is highest in regions where the amplitudes are below typical noise floors of present-day instruments. Similar to Constable & Weiss (2006), we estimate the noise floor (NF), for a recording system sensitivity V_r, receiver dipole length l_r, source current I, source length l_s and N_s-fold signal stacking, as $NF = V_r/(l_r I l_s \sqrt{N_s})$. For example, for a borehole source with $l_s = 150$ m and $I = 30$ A, a recording system with $V_r = 40$ nV, $l_r = 60$ m and $N_s = 1000$, we obtain $NF \approx 4.7 \times 10^{-15}$ V (Am^{-2}). We use instrument noise floors here to roughly assess (best-case) signal measurability for various source types, although in practise, noise floors are more likely determined by the level of cultural noise. At frequencies near 0.1–1 Hz and source–receiver distances of about 3–5 km, the electric field amplitudes exceed the theoretical noise floor and the sensitivities are still significantly higher than maximum sensitivities obtained for the surface sources. Provided that low-noise instrumentation and sufficient stacking is used, the reservoir should thus be better imageable by VED than by horizontal surface sources.

Normalized magnetic field sensitivities for the VED source are similar to electric field ones, with sensitivity to σ_v being much higher than that to σ_h. Unfortunately, the amplitudes of magnetic fields generated by VED sources are several orders of magnitude lower than for horizontal sources (compare contours in Figs 9b and 10c, d), and are below common instrument detection thresholds (using similar considerations as for the electric field, for magnetic field sensors having a noise level of $H_0 = 8.75 \times 10^{-8}$ A m^{-1} (at 1 Hz; Friedrichs 2010), we obtain $NF = H_0/(I l_s \sqrt{N_s}) \approx 6.2 \times 10^{-13}$ m^{-2}).

For magnetic sources and our land CSEM model, the EM field is practically only sensitive to the horizontal conductivity. In Fig. 11, we display sensitivities to the $\sigma_{h_{\mathrm{res}}}$ for a VMD source located at the surface. The fields for the unit dipole VMD are much smaller than those for the HED (compare contours in Figs 7 and 11). For the VMD source, we estimate the electric field noise floor as $NF = V_r/(l_r I a_z \sqrt{N_s})$ (the source dipole length used for HED noise floor estimation has been replaced by the loop area). For a loop area of 400×400 m^2, we obtain $NF \approx 1.4 \times 10^{-17}$ V (Am^{-2}). Similarly, we estimate the magnetic field noise floor to be $NF = H_0/(I a_z \sqrt{N_s}) \approx 1.8 \times 10^{-15}$ m^{-2}. Accordingly,

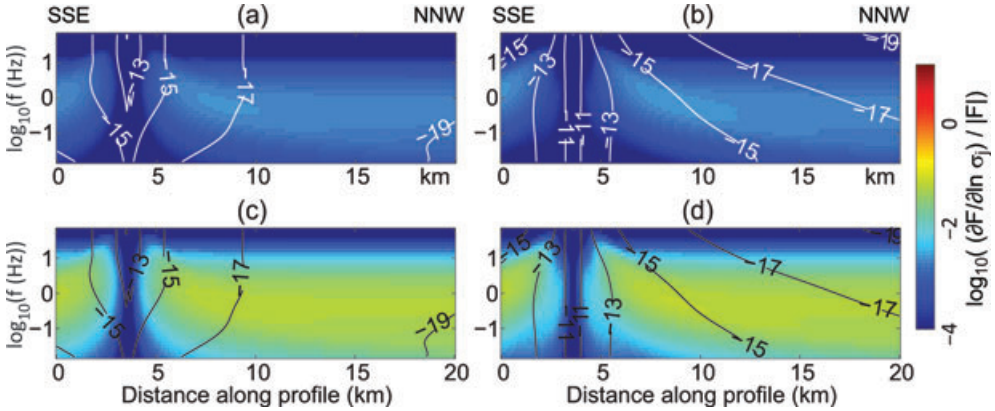

Figure 11. (a) E_y and (b) H_z sensitivity to the horizontal conductivity of the reservoir depicted in Fig. 6(a) for a VMD source located above the surface ($z = -0.1$ m). (c) E_y and (d) H_z sensitivities for the same source, but for a reservoir conductivity of 2.5 S m^{-1}.

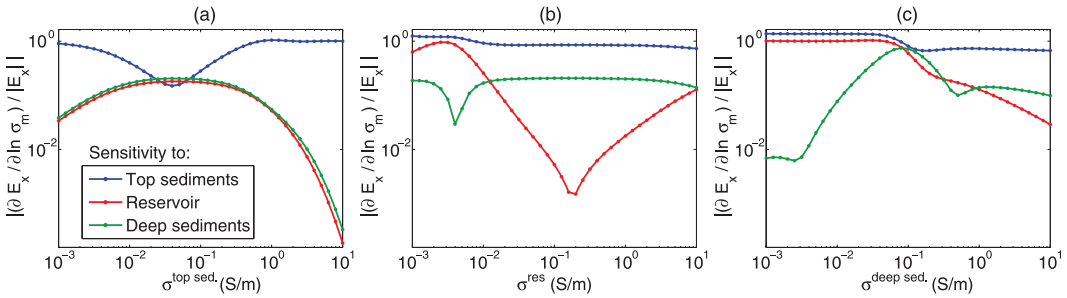

Figure 12. E_x sensitivity to each layer of the model from Fig. 6(a) for varying isotropic conductivity of (a) the top sediments, (b) the thin reservoir and (c) the deep sediments, for an x-directed HED source, a single inline receiver at 4 km offset and frequency 1 Hz.

regions of measurable electric and magnetic fields should be present in Fig. 11. Nonetheless, the normalized sensitivity to the resistor is very low at all frequencies and distances (Figs 11a and b). If the conductivity of the thin layer is increased to 2.5 S m^{-1}, the sensitivity increases markedly (Figs 11c and d) and may be sufficiently high to detect the layer. Sensitivity patterns for surface HMD sources are similar, but are not shown here, because an HMD source of similar dimensions as our VMD example would be impractical.

To investigate variations of sensitivity with varying conductivity, we display in Fig. 12 sensitivities to all layers at a single receiver location for wide ranges of overburden, reservoir and underburden conductivity. Obviously, conductivity variation in one layer induces strong non-linear changes of sensitivity not only to the layer in which conductivity changes, but also to all of the other layers. Sensitivity to the reservoir is minimal if the reservoir conductivity is slightly lower than that of the top sediments (Fig. 12b). For reservoir conductivities near 0.01 S m^{-1}, the reservoir exhibits maximum and the underlying unit minimum sensitivity. Here, the reservoir masks the deeper sediments. Sensitivity to the top sediments increases somewhat with decreasing reservoir conductivity. High sensitivity to the reservoir and top sediments appear to coincide. For lower reservoir conductivity, larger parts of the EM field are reflected back from the reservoir, leading to stronger overburden illumination that may also increase the sensitivity to the overburden. Sensitivity to the reservoir is high for overburden conductivities less than $\sim$0.05 S m^{-1} (Fig. 12c). Somewhat surprisingly, further reduction of overburden conductivity does not increase the sensitivity to the reservoir further.

For anisotropic conductivities, changes in horizontal conductivity may also influence the sensitivity to vertical conductivity, and vice versa (Fig. 13). For the example shown, horizontal conductivity of the reservoir $\sigma_{h_{\rm res}}$ correlates nearly linearly with sensitivity to $\sigma_{h_{\rm res}}$ and does not strongly influence the sensitivities to σ_h of the other layers and to σ_v (Figs 13a and b). In contrast, a minimum in sensitivity to horizontal conductivity of the deep sediments occurs for vertical reservoir conductivity near 0.004 S m^{-1} (Fig. 13c). Furthermore, for varying vertical reservoir conductivity, there is a striking correlation between sensitivities to σ_v of all layers, which is not present for isotropic conductivities (compare Figs 13d and 12b).

6 DISCUSSION AND CONCLUSIONS

We have presented an analytical formulation for EM field sensitivities for VTI-anisotropic layered media and various dipole and finite-length sources. This solution is quite general in that it permits arbitrary source and receiver depths. With a single trivial change, our expressions can identically be applied for computing sensitivities with respect to permittivity, which are of particular interest at high frequencies. Our explicit expressions are straightforward to implement and can be efficiently evaluated using fast Hankel transform filters. They should thus be useful for feasibility studies and experimental design of CSEM surveys, and can also be employed as a principal building block of EM inversion algorithms. Comparisons between analytical and numerical results have confirmed the validity of the analytic expressions. Such comparisons have also revealed that numerical solutions potentially are more prone to instability than the analytical ones, particularly when sensitivities are very low. In contrast, the analytical calculations produced stable results for all source–receiver configurations and models investigated. Furthermore, the analytical solution is significantly more efficient than finite-difference computations, with an even larger efficiency gain for VTI-anisotropic than for isotropic media.

Future work should include extensions for more general anisotropic conductivity. Although this is straightforward in principle, sensitivity computation for general anisotropy will be significantly more costly. The sensitivity expressions will become more complex, involving cross-coupling terms between the TE and TM modes (Løseth & Ursin 2007). Therefore, reduction to Hankel integrals as in the VTI case will no longer be possible.

A feasibility study for CSEM characterization of a carbon sequestration site has demonstrated the usefulness of sensitivity computations and the capability of handling complex realistic source geometries. For the site studied, an important result was that a combination of surface-based and borehole-to-surface measurements likely is best-suited for imaging both the larger-scale structure and the reservoir rock. The vertical conductivity of the thin reservoir is well resolved by the electric fields generated by electric sources. The horizontal conductivity of the resistive reservoir is poorly resolved by all source types and field components, whereas the horizontal conductivity of a thin good conductor in the place of the resistor would be significantly better resolved, particularly by the magnetic field. Accordingly, by exploiting

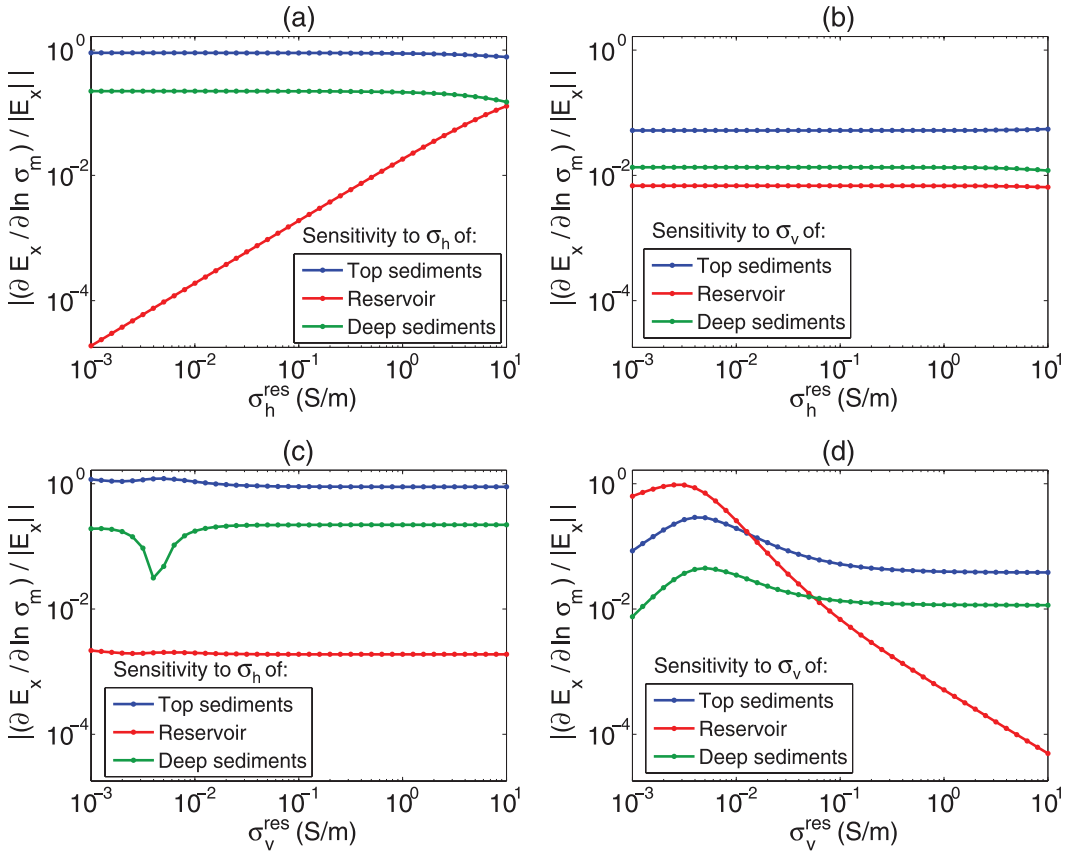

Figure 13. E_x sensitivity to each layer of the model from Fig. 6(a) for variable horizontal and vertical reservoir conductivity $\sigma_{h_{\text{res}}}$ and $\sigma_{v_{\text{res}}}$. We display the sensitivities to (a) horizontal and (b) vertical conductivity for variable $\sigma_{h_{\text{res}}}$, and sensitivities to (c) horizontal and (d) vertical conductivity for variable $\sigma_{v_{\text{res}}}$.

complementary sensitivity properties of different EM field components and jointly using electric and magnetic fields within EM inversion, the VTI anisotropy of thin conductors may well be resolvable.

More generally, sensitivity patterns appear to coincide broadly with the direction of current flow. Horizontal currents, which determine the magnetic field at the surface, primarily exhibit high sensitivity to good conductors. Accordingly, the magnetic field at the surface is primarily sensitive to the horizontal conductivity and resolves good conductors much better than resistive layers. Vertical currents, which primarily determine the TM-mode fields, are mainly sensitive to poor conductors that limit current flow. At the surface, TM-mode contributions are practically only contained in the electric field, such that only the electric field is sensitive to the vertical conductivity. Vertical electric sources generate particularly large components of vertical current flow. As a result, the EM field for VED sources is primarily sensitive to σ_v.

Analysis of sensitivity as a function of conductivity may provide additional information for assessing CSEM exploration and monitoring feasibility, because the relation between sensitivity and conductivity is highly non-linear, and conductivity changes in one layer may strongly influence the sensitivities to the entire conductivity structure.

ACKNOWLEDGMENTS

This work was funded by the German Federal Ministry of Education and Research within the framework of the GeoEn project. Constructive comments by two anonymous reviewers helped improve the manuscript.

REFERENCES

Abubakar, A., Liu, J., Li, M., Habashy, T. & MacLennan, K., 2010. Sensitivity study of multi-sources receivers CSEM data for TI-anisotropy medium using 2.5D forward and inversion algorithm, in *Proceedings of the 72nd EAGE Conference,* Barcelona, Extended Abstract.

Anderson, W.L., 1982. Fast Hankel transforms using related and lagged convolutions, *ACM Trans. Math. Softw.,* **8**(4), 344–368.

Andréis, D. & MacGregor, L., 2008. Controlled-source electromagnetic sounding in shallow water: principles and applications, *Geophysics,* **73**(1), F21–F32.

Chave, A.D., 1983. Numerical integration of related Hankel transforms by quadrature and continued fraction expansion, *Geophysics,* **48**(12), 1671–1686.

Chave, A.D., 1984. The fréchet derivatives of electromagnetic induction, *J. geophys. Res.,* **89**(B5), 3373–3380.

Chave, A.D., 2009. On the electromagnetic fields produced by marine frequency domain controlled sources, *Geophys. J. Int.,* **179**, 1429–1457.

Chave, A.D. & Cox, C.S., 1982. Controlled electromagnetic sources for measuring electrical conductivity beneath the oceans, 1. forward problem and model study, *J. geophys. Res.,* **87**(B7), 5327–5338.

Christensen, N.B., 1990. Optimized fast Hankel transform filters, *Geophys. Prospect.,* **38**, 545–568.

Commer, M. & Newman, G.A., 2008. New advances in three-dimensional controlled-source electromagnetic inversion, *Geophys. J. Int.,* **172**, 513–535.

Constable, S. & Weiss, C.J., 2006. Mapping thin resistors and hydrocarbons with marine EM methods: insights from 1D modeling, *Geophysics,* **71**(2), G43–G51.

Constable, S.C., Parker, R.L. & Constable, C.G., 1987. Occam's inversion: a practical algorithm for generating smooth models from electromagnetic sounding data, *Geophysics,* **75**(3), 289–300.

Eidesmo, T., Ellingsrud, S., MacGregor, L. M., Constable, S., Sinha, M. C., Johansen, S., Kong, F. N. & Westerdahl, H., 2002. Sea Bed Logging (SBL), a new method for remote and direct identification of hydrocarbon filled layers in deepwater areas, *First Break,* **20**(3), 144–152.

Everett, M.E. & Constable, S., 1999. Electric dipole fields over an anisotropic sea£oor: theory and application to the structure of 40 Ma Pacific Ocean lithosphere, *Geophys. J. Int.,* **136**, 41–56.

Farquharson, C.G. & Oldenburg, D.W., 1996. Approximate sensitivities for the electromagnetic inverse problem, *Geophys. J. Int.,* **126**, 235–252.

Ferguson, I.J. & Edwards, R.N., 1994. Electromagnetic mode conversion by surface-conductivity anomalies: applications for conductivity soundings, *Geophys. J. Int.,* **117**, 48–68.

Flosadóttir, A.H. & Constable, S., 1996. Marine controlled-source electromagnetic sounding – 1. Modeling and experimental design, *J. geophys. Res.,* **101**(B3), 5507–5517.

Friedrichs, B., 2010. *Product Memo: MFS-06e Broad Band Induction Coil Magnetometer,* Metronix Messgeraete und Elektronik GmbH, Braunschweig, Germany.

Giese, R. *et al*., 2009. Monitoring at the CO_2SINK site: a concept integrating geophysics, geochemistry and microbiology, *Energy Procedia,* **1**(1), 2251–2259.

Haber, E., Oldenburg, D.W. & Shekhtman, R., 2007. Inversion of time domain three-dimensional electromagnetic data, *Geophys. J. Int.,* **171**, 550–564.

Johansen, H.K. & Sørensen, K., 1979. Fast Hankel transforms, *Geophys. Prospect.,* **27**, 876–901.

Key, K., 2009. 1D inversion of multicomponent, multifrequency marine CSEM data: methodology and synthetic studies for resolving thin resistive layers, *Geophysics,* **74**(2), F9–F20.

Løseth, L.O., 2011. Insight into the marine controlled-source electromagnetic signal propagation, *Geophys. Prospect.,* **59**, 145–160.

Løseth, L.O. & Ursin, B., 2007. Electromagnetic fields in planarly layered anisotropic media, *Geophys. J. Int.,* **170**, 44–80.

Newman, G.A. & Alumbaugh, D.L., 1997. Three-dimensional massively parallel electromagnetic inversion - I. Theory, *Geophys. J. Int.,* **128**, 345–354.

Newman, G.A. & Boggs, P.T., 2004. Solution accelerators for large-scale three-dimensional electromagnetic inverse problems, *Inverse Prob.,* **20**, S151–S170.

Newman, G.A., Commer, M. & Carazzone, J.J., 2010. Imaging CSEM data in the presence of electrical anisotropy, *Geophysics,* **75**(2), F51–F61.

Orange, A., Key, K. & Constable, S., 2009. The feasibility of reservoir monitoring using time-lapse marine CSEM, *Geophysics,* **74**(2), F21–F29.

Piessens, R., de Doncker-Kapenga, E., Überhuber, C.W. & Kahaner, D., 1983. *QUADPACK: A Subroutine Package for Automatic Integration,* Springer, Berlin.

Press, W.H., Teukolsky, S.A., Vetterling, W.T. & Flannery, B.P., 1992. *Numerical Recipes in Fortran 77,* 2nd edn, Vol. 1, Cambridge University Press, New York, NY.

Ridders, C.J.F., 1982. Accurate computation of f'(x) and f'(x) f''(x), *Adv. Eng. Softw.,* **4**(2), 75–76.

Streich, R. & Becken, M., 2011. Electromagnetic fields generated by finite-length wire sources: comparison with point dipole solutions, *Geophys. Prospect.,* **59**, 361–374.

Streich, R., Becken, M. & Ritter, O., 2010. Imaging of CO_2 storage sites, geothermal reservoirs, and gas shales using controlled-source magnetotellurics: modeling studies, *Chemie der Erde (Geochemistry),* **70**(S3), 63–75.

Um, E.S. & Alumbaugh, D.L., 2007. On the physics of the marine controlled-source electromagnetic method, *Geophysics,* **72**(2), WA13–WA26.

Ward, S.H. & Hohmann, G.W., 1987. Electromagnetic theory for geophysical applications, in *Electromagnetic Methods in Applied Geophysics,* pp. 131–311, ed. Nabighian, M.N., Society of Exploration Geophysicists.

Weidelt, P., 2007. Guided waves in marine CSEM, *Geophys. J. Int.,* **171**, 153–176.

Wirianto, M., Mulder, W.A. & Slob, E.C., 2010. A feasibility study of land CSEM reservoir monitoring in a complex 3-D model, *Geophys. J. Int.,* **181**, 741–755.

Zhdanov, M.S., 2009. New advances in regularized inversion of gravity and electromagnetic data, *Geophys. Prospect.,* **57**, 463–478.

Ziolkowski, A., Parr, R., Wright, D., Nockles, V., Limond, C., Morris, E. & Linfoot, J., 2010. Multi-transient electromagnetic repeatability experiment over the North Sea Harding field, *Geophys. Prospect.,* **58**, 1159–1176.

APPENDIX: ISOTROPIC EXPRESSIONS

EM field sensitivities for isotropic media are obtained by making small modifications to the expressions given in Section 4. Taking $\tilde{\varepsilon}_{h_m} = \tilde{\varepsilon}_{v_m} = \tilde{\varepsilon}_m$, the vertical slowness becomes $p_{z_m}^{TE} = p_{z_m}^{TM} = p_{z_m} = \sqrt{\mu_0\tilde{\varepsilon}_m - p_h^2}$. Then the derivatives of the isotropic reflection and transmission coefficients are for layer boundary m (see eq. 14)

$$\frac{\partial \acute{r}_m^{TE}}{\partial \tilde{\varepsilon}_m} = \frac{-\mu_0 \acute{t}_m^{TE}\grave{t}_m^{TE}}{4p_{z_m}^2}, \quad \frac{\partial \grave{r}_m^{TE}}{\partial \tilde{\varepsilon}_m} = -\frac{\partial \acute{r}_m^{TE}}{\partial \tilde{\varepsilon}_m},$$
$$\frac{\partial \acute{t}_m^{TE}}{\partial \tilde{\varepsilon}_m} = \frac{\mu_0 \acute{t}_m^{TE}\acute{r}_m^{TE}}{4p_{z_m}^2}, \quad \frac{\partial \grave{t}_m^{TE}}{\partial \tilde{\varepsilon}_m} = \frac{\partial \acute{t}_m^{TE}}{\partial \tilde{\varepsilon}_m}, \tag{A1a}$$

$$\frac{\partial \acute{r}_m^{TM}}{\partial \tilde{\varepsilon}_m} = \frac{-\left(2p_{z_m}^2 - \mu_0\tilde{\varepsilon}_m\right)\acute{t}_m^{TM}\grave{t}_m^{TM}}{4p_{z_m}^2\,\tilde{\varepsilon}_m}, \quad \frac{\partial \grave{r}_m^{TM}}{\partial \tilde{\varepsilon}_m} = -\frac{\partial \acute{r}_m^{TM}}{\partial \tilde{\varepsilon}_m},$$
$$\frac{\partial \acute{t}_m^{TM}}{\partial \tilde{\varepsilon}_m} = \frac{\left(2p_{z_m}^2 - \mu_0\tilde{\varepsilon}_m\right)\acute{t}_m^{TM}\acute{r}_m^{TM}}{4p_{z_m}^2\,\tilde{\varepsilon}_m}, \quad \frac{\partial \grave{t}_m^{TM}}{\partial \tilde{\varepsilon}_m} = \frac{\partial \acute{t}_m^{TM}}{\partial \tilde{\varepsilon}_m}, \tag{A1b}$$

and analogous for layer boundary $m-1$.

Upward reflection is described by eqs. (18), (22) and (23), with the factor C_1

$$C_1 = \frac{\mathrm{i}\omega\mu_0 d_m}{p_{z_m}} \tag{A2a}$$

for both the TE and TM mode reflection responses. The factor C_2 is

$$C_2 = \frac{\mu_0}{4p_{z_m}^2} \tag{A2b}$$

for the TE-mode response and

$$C_2 = \frac{2p_{z_m}^2 - \mu_0\tilde{\varepsilon}_m}{4p_{z_m}^2\tilde{\varepsilon}_m} \tag{A2c}$$

for the TM-mode response.

Substituting these factors into eqs (26), (29) and (31)–(36) results in the isotropic derivatives of the upward transmission and downward reflection and transmission responses.

The TE-mode derivatives of the isotropic integral kernels are the same as eqs (41a), (42a), (43a) and (44a), with $\tilde{\varepsilon}_{h_m}$ and $p_{z_m}^{TE}$ replaced by the isotropic $\tilde{\varepsilon}_m$ and p_{z_m}. The derivatives of the TM-mode integral kernels are similar to eqs (41b), (42b), (43b) and (44b), with the substitutions $\tilde{\varepsilon}_{h_m} \rightarrow \tilde{\varepsilon}_m$, $\partial_{z_m}^{TM} \rightarrow \partial_{z_m}$ and

$$\left(\frac{1}{\tilde{\varepsilon}_{h_m}} - \frac{\mu_0 - \frac{p_h^2}{\tilde{\varepsilon}_{v_m}}}{2p_{z_m}^{TM^2}}\right) \rightarrow \left(\frac{1}{\tilde{\varepsilon}_m} - \frac{\mu_0}{2p_{z_m}^2}\right).$$

The isotropic expressions for the derivatives of the EM field components are nearly identical to the derivatives with respect to $\tilde{\varepsilon}_{h_m}$ given in eqs (46), (48), (50), (52) and (53), with one exception: all instances of $\tilde{\varepsilon}_{v_m}$ appearing in the coefficients in front of the integrals for E_z for HED, HMD and long wire sources (eqs 2c, 8c and 12c), and in front of all integrals for VED sources (eq. 10), are replaced by the isotropic $\tilde{\varepsilon}_m$. Accordingly, the extra terms for the source and receiver layers appearing in the $\tilde{\varepsilon}_{v_m}$ derivatives in eqs (47c), (49c) and (51) are also contained in the isotropic sensitivity expressions. For example, the isotropic E_z sensitivity for an HED source is

$$\frac{\partial E_z}{\partial\tilde{\varepsilon}_m} = \delta_{Rm}\left(-\frac{Il_x}{4\pi}\frac{\mathrm{i}\cos\beta}{\omega\tilde{\varepsilon}_R^2}\int_0^\infty \kappa^2 J_1(\kappa r) g_D^{TM}\mathrm{d}\kappa\right) + \frac{Il_x}{4\pi}\frac{\mathrm{i}\cos\beta}{\omega\tilde{\varepsilon}_R}\int_0^\infty \kappa^2 J_1(\kappa r)\frac{\partial g_D^{TM}}{\partial\tilde{\varepsilon}_m}\mathrm{d}\kappa. \tag{A3}$$